

Instituto Tecnológico de Costa Rica

Escuela de Ingeniería en Electrónica

“Design, Simulation and Validation of an Equivalent Circuit Model  
for a Valveless Piezoelectric Micropump”

para optar por el título de

Magister Scientiae en Electrónica

con énfasis en Sistemas Microelectromecánicos

con el grado académico de

Maestría

Juan José Rojas Hernández

Cartago, Agosto, 2016.

I declare that this thesis document has been done fully by myself, using and applying related literature and adding own knowledge and experimental results. In the cases I used literature I cited it in a proper way. Consequently, I take full responsibility for this work and the contents of this document.

Juan José Rojas Hernández

ID: 3-0391-0836

Cartago, 24th August, 2016

This work is licensed under a [Creative Commons](#)  
“Attribution-NonCommercial-ShareAlike 4.0 International” license.





Instituto Tecnológico de Costa Rica  
Escuela de Ingeniería Electrónica  
Tesis de Maestría  
Tribunal evaluador

Tesis de maestría defendida ante el presente Tribunal Evaluador como requisito para optar por el grado académico de maestría, del Instituto Tecnológico de Costa Rica.

Miembros del Tribunal



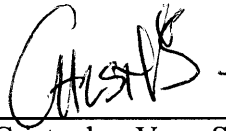
---

Máster Luis Diego Murillo Soto  
**Profesor lector**



---

M.Sc. Gustavo Richmond Navarro  
**Profesor lector**



---

M.Sc. Cristopher Vega Sánchez  
**Director de Tesis**

Los miembros de este Tribunal dan fe de que la presente tesis ha sido aprobada y cumple con las normas establecidas por la Escuela de Ingeniería Electrónica.

Cartago, 24 de agosto de 2016

To my wife María and my son Samuel.

## ACKNOWLEDGMENTS

The author wants to thank Instituto Tecnológico de Costa Rica for grant an scholarships for the complete Master's program and the Council of the Electromechanical Engineering School for approving the participation in this scholarship.

The author wants to thanks to Christopher Vega for his continuous support during the development of this work.

Special thanks to Victor Alfaro for kindly answering multiple questions about the Generalized Network theory.

## PREFACE

This thesis is submitted in partial fulfillment of the requirements for a Master of Science Degree in Electronics with emphasis in Microelectromechanical Systems of Instituto Tecnológico de Costa Rica. It contains work done from September of 2015 to August of 2016.

In June of 2015, one of my colleagues introduce me to the *Generalized Network*, a theory developed by Prof. Victor M. Alfaro at Universidad de Costa Rica, this theory applies the laws and theorems of electric circuits to other dynamic systems that can be represented using the elements of these networks. The possibility of using the properties of the electrical circuits to describe and analyze dynamic systems was attractive to me, since I have been teaching on electric circuits for a couple of semesters. At the same time, while doing research for a course project, I came across with different configurations and actuation methods of micropumps, one of them attracted me for its simplicity: the valveless micropump.

For those reasons I decided to define an equivalent electric circuit for a piezoelectric valveless micropump and validate the model using both a fabricated prototype and FEM simulations. An idea was born, this work is the result of following that idea.

During the development of the research proposal, I noticed that, in the available literature, some researchers used FEM simulation to determine the behavior of a part of the system they were analyzing and present those results alone, without integrating them into the system. Other authors use completely analytical determined models and then validate them using experimental results, FEM simulations or both. What if, instead of that, a complete model is built with lumped blocks –subsystems–, that are in some way independent, and each of them is defined using FEM simulations or analytic solutions depending of each case. I decided to develop this approach as the main contribution of my thesis.

## TABLE OF CONTENTS

	Page
LIST OF TABLES . . . . .	x
LIST OF FIGURES . . . . .	xi
NOMENCLATURE . . . . .	xiii
GLOSSARY . . . . .	xvi
ABSTRACT . . . . .	xvii
1 Introduction . . . . .	1
1.1 Context . . . . .	1
1.2 Problem . . . . .	1
1.3 Hypothesis . . . . .	2
1.4 Objectives . . . . .	2
1.4.1 General objective . . . . .	2
1.4.2 Specific objectives . . . . .	2
1.5 Research Method . . . . .	3
1.6 Structure of the Thesis . . . . .	3
2 Theoretical framework. . . . .	6
2.1 Schematic and principle of operation of the PVM . . . . .	6
2.2 Solid mechanics: elasticity . . . . .	7
2.3 Electrostatics: Piezoelectric effect . . . . .	9
2.4 Fluid dynamics: Poiseuille flow . . . . .	10
2.4.1 Navier-Stokes equations . . . . .	11
2.4.2 Continuity equation . . . . .	11
2.4.3 Hagen–Poiseuille equation . . . . .	12
2.4.4 Pressure loss in Poiseuille flow . . . . .	14
2.5 Dynamic system modeling: Equivalent electric circuits . . . . .	16

	Page
2.5.1 Electrical Equivalent Networks for Fluid Dynamics Modeling	19
3 Piezoelectric Valveless Micropump Equivalent Circuit Model . . . . .	22
3.1 Geometry of the micropump . . . . .	22
3.2 Overview of the system . . . . .	23
3.3 Determination of output parameters of lumped elements . . . . .	25
3.3.1 Piezoelectric actuator model . . . . .	25
3.3.2 Chamber . . . . .	29
3.4 Inlet and outlet . . . . .	31
3.4.1 Inlet and Outlet water columns . . . . .	36
3.5 Model simulation . . . . .	37
4 Equivalent circuit model validation . . . . .	39
4.1 FEM Simulation . . . . .	39
4.2 Fabricated prototype . . . . .	42
4.3 Results comparison and discussion . . . . .	46
5 Conclusion and outlook . . . . .	51
5.1 Conclusion . . . . .	51
5.2 Outlook . . . . .	52
REFERENCES . . . . .	53
A Datasheets . . . . .	54

## LIST OF TABLES

Table	Page
2.1 Values of $k_g$ for different geometries. . . . .	15
2.2 Transvariables and pervariables of dynamic systems. . . . .	18
2.3 Constitutive relation and generalized impedance of the basic elements.	19
3.1 Input parameters of lumped elements. . . . .	23
3.2 Simulation configurations for actuator. . . . .	28
3.3 Geometric parameters for simulations. . . . .	32
3.4 Simulation configurations for nozzles and diffusers. . . . .	33
3.5 Simulation results for hydraulic resistances. . . . .	36
4.1 Simulation configurations for complete PVM. . . . .	41
4.2 Simulation results for complete PVM. . . . .	42
4.3 Quantitative comparison. . . . .	49
4.4 Solution time comparison. . . . .	49
4.5 Qualitative comparison for the PVM . . . . .	50

## LIST OF FIGURES

Figure	Page
1.1 Structure of the thesis . . . . .	5
2.1 Assembly of the piezoelectric valveless micropump . . . . .	6
2.2 Principle of operation of PVM. . . . .	7
2.3 Schematic of the actuation system . . . . .	10
2.4 Arbitrary flow streamtube . . . . .	12
2.5 Poiseuille flow in a pipe . . . . .	13
2.6 Schematic of an energy port . . . . .	18
3.1 Geometry of the micropump. . . . .	22
3.2 Equivalent circuit model. . . . .	24
3.3 Axisymmetric geometry of actuator. . . . .	25
3.4 Waveforms of input $u(t)$ , and output $y(t)$ , obtained from the simulation	27
3.5 Geometrical approximation of the chamber. . . . .	30
3.6 Variable hydraulic resistance diagram . . . . .	32
3.7 Curves for $\mathcal{R}'_{cid}/\mathcal{R}'_{cod}$ and $\mathcal{R}'_{cis}/\mathcal{R}'_{cos}$ for different values of Reynolds number	34
3.8 Curves for $\mathcal{R}''_{cod}$ and $\mathcal{R}''_{cos}$ for different values of Reynolds number . . . .	34
3.9 Values for $\mathcal{R}''_{cid}$ and $\mathcal{R}''_{cis}$ for different values of Reynolds number . . . .	34
3.10 Curves for $\mathcal{R}'_{oud}$ and $\mathcal{R}'_{ous}$ for different values of Reynolds number . . . .	35
3.11 Curves for $\mathcal{R}'_{ind}$ and $\mathcal{R}'_{ins}$ for different values of Reynolds number . . . .	35
3.12 Top view of the connection between inlet and outlet port with needle tip	35
3.13 Implemented simulink model. . . . .	38
4.1 Geometry used in COMSOL for PVM. . . . .	40
4.2 Fabricated prototype. . . . .	43
4.3 Experimental setup with a prototype on place. . . . .	44
4.4 Pumped volume over time . . . . .	47

4.5 Characteristic curve of PVM . . . . . 48

## NOMENCLATURE

$\epsilon$	Unit strain []
$\lambda$	Lamé's first parameter [Pa], second viscosity coefficient [Pa]
$\mathbf{f}$	Body force vector [ $\text{N m}^{-3}$ ]
$\mathbf{u}$	Velocity vector [ $\text{m s}^{-1}$ ], displacement vector [m]
$\mathcal{C}$	Compliance [ $\text{m}^3 \text{Pa}^{-1}$ ]
$\mathcal{L}$	Inertance [ $\text{Pa s}^2 \text{m}^{-3}$ ]
$\mathcal{L}$	Laplace transform
$\mathcal{R}$	Hydraulic resistance [ $\text{Pa s m}^{-3}$ ]
$\mathcal{V}$	Volume [ $\text{m}^3$ ]
$\mathcal{Z}$	Impedance operator [ $\text{m}^3$ ]
$\mu$	Shear modulus [Pa], dynamic viscosity [ $\text{N s m}^{-2}$ ]
$\nabla$	Nabla operator
$\mathcal{D}$	Differential operator
$f$	Rate pervariable
$h$	State pervariable
$v$	Rate transvariable

$\chi$	State transvariable
$\omega$	Angular frequency [ $\text{rad s}^{-1}$ ]
$\rho$	Density [ $\text{kg m}^{-3}$ ]
$\sigma$	Unit stress [ ]
$v$	Average velocity [ $\text{m s}^{-1}$ ]
$a$	Width of the rectangular pipe or channel [m]
$a_r$	Aspect ratio, $a/b$ [ ]
$b$	Height of the rectangular pipe or channel [m]
$D_H$	Hydraulic diameter [m]
$E$	Electric field [ $\text{Vm}^{-1}$ ]
$f$	Body force vector component [ $\text{N m}^{-3}$ ]
$k_g$	Geometry factor [ ]
$K_x$	Resistance coefficient [ ]
$L_e$	Equivalent length, $L/D$ [m]
$m$	Mass [ kg]
$p$	Pressure [Pa]
$Q$	Flow rate [ $\text{m}^2\text{s}^{-1}$ ]
$R$	Electric resistance [ $\Omega$ ]
$R$	Specific gas constant [ $\text{J kg}^{-1} \text{K}^{-1}$ ]
$Re$	Reynolds number [ ]

$T$	Temperature [K]
$u$	Velocity vector component [ $\text{m s}^{-1}$ ], displacement vector component [m]
$V$	Voltage [V]
$W_P$	Wetted perimeter [m]
$T$	Period of a wave [ $\text{s}^{-1}$ ]

## GLOSSARY

PZT	It refers to the piezoceramic material called PZT-5H (Lead Zirconate Titanate)
FEM	Finite Element Method
PVM	Piezoelectric Valveless Micropump
HECM	Hybrid Equivalent Electric Circuit Model
GAG	Glass-adhesive-glass fabrication technique
LTI	Linear time-invariant system
ODE	Ordinary differential equation

## ABSTRACT

Rojas, Juan J. , Instituto Tecnológico de Costa Rica, August 2016. Design, Simulation and Validation of an Equivalent Circuit Model for a Valveless Piezoelectric Micropump. Thesis Director: M.Sc. Cristopher Vega Sanchez.

Equivalent electric circuit models are commonly used in microfluidics to represent the dynamic behavior of fluidic components in terms of their equivalent electric counterparts.

FEM simulation tools are widely used for solving complicated problems, usually involving coupled physics.

In this work a *hybrid electric circuit model* –HECM– and a complete *FEM simulation* are used to characterize a piezoelectric valveless micropump –PVM–. The model is considered *hybrid* because the parameters of the lumped elements are obtained using analytic solutions or FEM simulations depending of each case.

Results of those two approaches – HECM and FEM simulations– are compared to experimental results obtained from the fabrication of a number of equal prototypes. The prototypes are fabricated using a technique called *GAG* –glass adhesive glass– which uses a combination of glass and adhesive layers to create a flow path.

The HECM was 5 times faster in obtaining the required results and it was more accurate to describe the behavior of the PVM.

**Keywords:** equivalent circuit models, piezoelectric, valveless, micropump.

# 1. INTRODUCTION

## 1.1 Context

The Microfluidics Laboratory of the School of Electromechanical Engineering is an ambitious new project whose goal is to produce low-cost microfluidic devices for different applications.

The research group is currently working on several projects:

- Electric impedance spectroscopy of cells.
- Effectiveness of adhesive strength on glass substrates for low-cost fabrication microfluidics: Blister test of selected adhesives.
- Valveless micropump: characterization, integration and packaging.

Most of the experiments to be done in the future will require a micropump to drive the fluid. Also the pulsatile nature of the pump can be used to obtain dynamic properties of different channels, accessories or tubings.

## 1.2 Problem

FEM simulation tools are widely used for solving complicated problems, usually involving coupled physics. Most FEM models are three dimensional and this increase the complexity of the mesh and elevate the computational cost. For those reasons, a complete simulation –that include the parts that are well characterized by analytic theories– is not the best approach.

In this context, dynamics systems modeling techniques are necessary to develop the complete system as a network of subsystems which exchange energy. Once the

subsystems are defined, it has to be determined whether is convenient to use a simulation result or an analytic solution to characterize this subsystem –also known as *lumped element*–. When all these lumped elements are fully described the complete system can be efficiently characterized.

### 1.3 Hypothesis

A model built using electrical networks equivalent elements whose parameters are determined by means of analytic solutions or FEM simulations depending on each case –Hybrid Equivalent Electric Circuit Model or HECM–, is more convenient for characterization purposes over a complete FEM simulation of the system, in terms of demand of computing resources, time and ease of implementation.

### 1.4 Objectives

#### 1.4.1 General objective

- Demonstrate the advantages of an HECM over a complete FEM simulation by comparing their efficiency in successfully characterizing a PVM.

#### 1.4.2 Specific objectives

- Develop a model of the PVM using electrical equivalent lumped elements.
- Determine the parameters of the model lumped elements using FEM simulations or analytical solutions.
- Simulate the complete PVM using FEM software.
- Build a functional prototype of the PVM using a low-cost fabrication technique to validate the model.
- Compare the efficiency and validity of the two solutions.

## 1.5 Research Method

To achieve the proposed objectives, the following steps will be carried out:

1. Literature review: basic theoretical concepts needed to understand the principle behind the operation of the micropump.
2. Evaluation and determination of the required lumped elements to successfully model the system.
3. Parameter determination using the best approach –analytical solution or FEM simulation– for each lumped element.
4. Set and run the model using an electrical simulation tool and obtain the results.
5. Develop and configure a FEM simulation of the complete micropump. Run it and obtain the results.
6. Build a functional prototype of the mPVM using the GAG technique. Set the experiment and measure, obtain the results.
7. Compare the results with the experimental data for validation, and compare solution time for each method to evaluate efficiency.
8. Analyze data and conclude.

## 1.6 Structure of the Thesis

This document is a selection of the most relevant work carried out during the development of the thesis. There is a lot of information that was left out, most of it, is well documented in the *log notebook* or in scripts files.

Chapter 2 presents the theoretical framework upon which the rest of this work was done. The governing equations of fluid flow, plate bending, and piezoelectric effect are introduced. Equivalent circuit theory is presented and fluid dynamics modeling

using this theory is further explored. At the end of this chapter, a *state of the art* review is done.

Chapter 3 shows, step by step, the process for determining the HECM of the PVM. In some cases the parameters are determined using both analytic solutions and FEM simulations in order to show which approach is better for each case.

Chapter 4 presents the validation of the ECM for the PVM using both FEM simulations and a fabricated prototype.

Chapter 5 is dedicated to conclusions with a small reference to future work.

A schematic of the described structure is shown in Fig. 1.1.

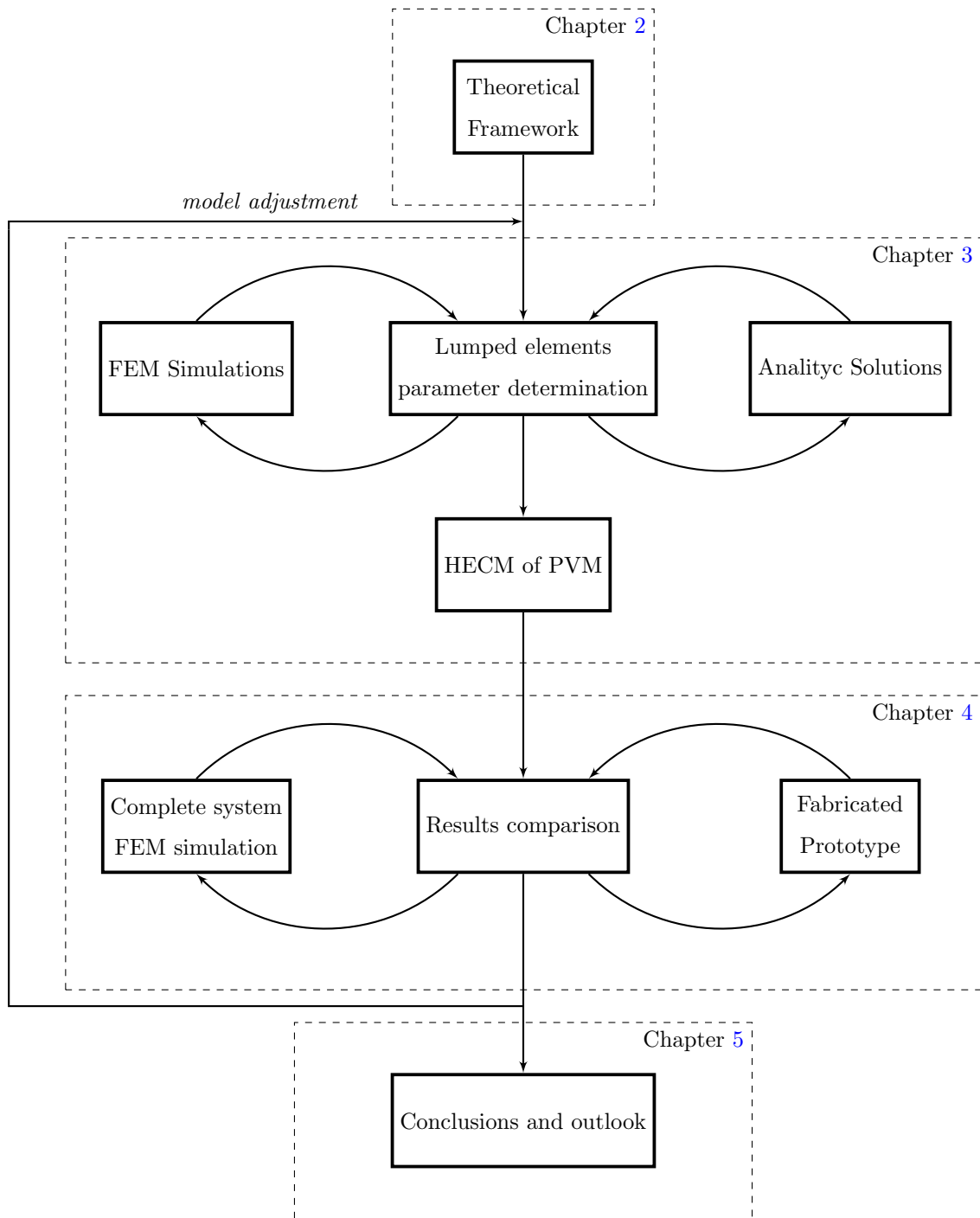


Fig. 1.1.: Structure of the thesis

## 2. THEORETICAL FRAMEWORK.

An schematic and a review of the principle of operation of the PVM is covered in Section 2.1, this principle involves multiple phenomena that includes solid mechanics, electrostatics and fluid dynamics. These subjects are covered in Sections 2.2 to 2.4.

Dynamic system modeling basics is covered in Section 2.5. A special focus on fluid dynamics modeling using equivalent electrical circuits can be found in Section 2.5.1.

### 2.1 Schematic and principle of operation of the PVM

The PVM consist of a patterned adhesive enclosed between two borosilicate glasses, actuated using a piezoelectric buzzer glued to the thinner glass. Details are shown in Fig 2.1. A more detailed overview of the fabrication technique can be found in Section 4.2.

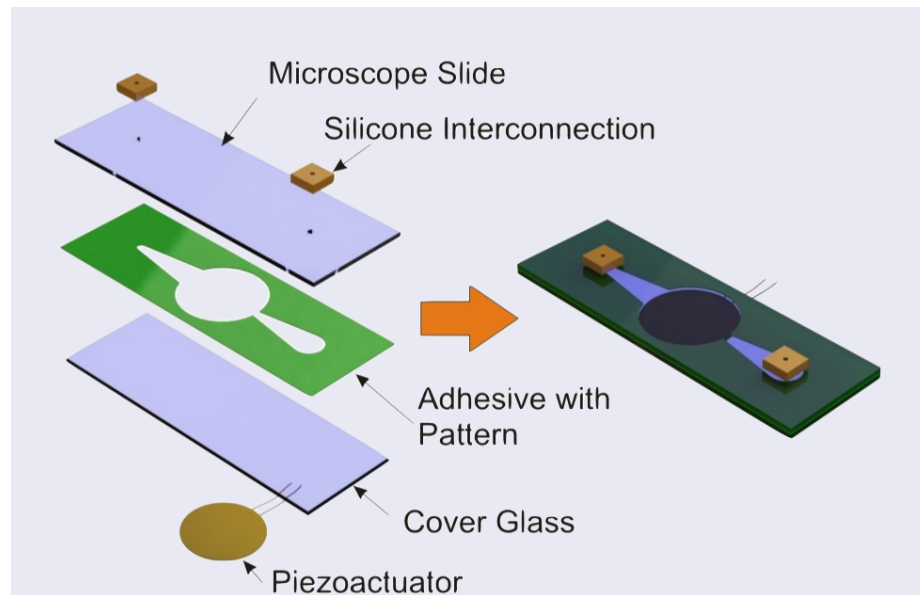


Fig. 2.1.: Assembly of the piezoelectric valveless micropump

The basic principle behind the operation of this pump is the differences between pressure losses in the inlet and outlet ports, both are of the nozzle/diffuser kind. The way this port behaves depends of the flow direction on each instant, so each port behave as a nozzle when the flow is entering in the larger area and like a diffuser when the flow is entering the smaller area. Under laminar flow regime the pressure drop is bigger for a nozzle that for a diffuser, assuming a similar geometry. Taking this into account it is clear that when the membrane move upward the fluid is absorbed on both ends, but the pressure drop on the outlet is bigger, because it is acting as a nozzle. As a consequence there is a larger volume of fluid being absorbed in the inlet in comparison with the outlet, as shown in Fig. 2.2a. On the other hand, when the membrane is moving downward, the opposite will occur, now the inlet is acting as a nozzle, having a larger pressure drop, thus the larger volume is being expelled in the outlet as shown in Fig. 2.2b.

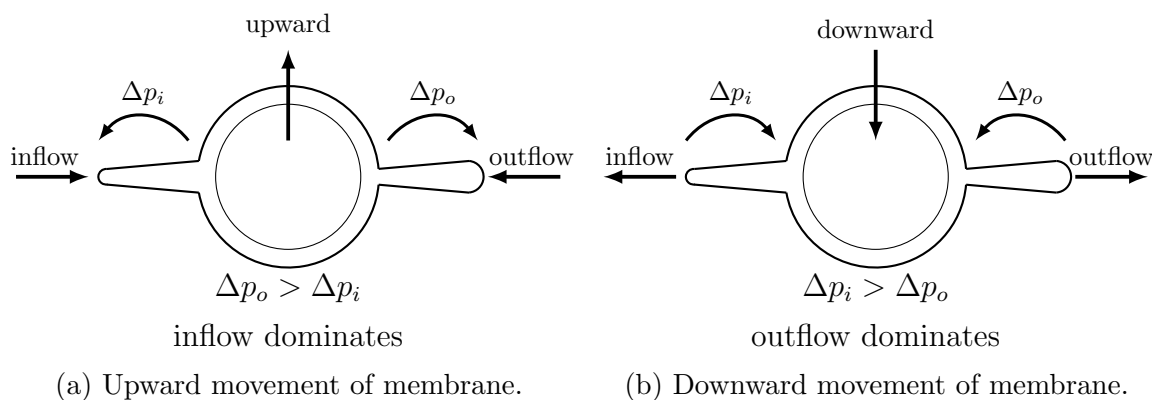


Fig. 2.2.: Principle of operation of PVM.

## 2.2 Solid mechanics: elasticity

The elasticity of a solid is characterized in terms of *stress* and *strain*. These terms are defined below [1].

**Stress:** internal force exerted by either of two adjacent parts of a body upon the other, across an imagined plane of separation.

**Strain:** a forced change in the dimensions of a body.

The application of Newton's second law to a solid volume yields to:

$$\rho \frac{\partial^2 u_i}{\partial t^2} = \frac{\partial \sigma_{ij}}{\partial x_j} + f_i, \quad (2.1)$$

where  $\rho$  is the density of the solid,  $u_i$  is the  $i$ th component of the displacement vector,  $\sigma_{ij}$  is the stress tensor, and  $f_i$  is the  $i$ th component of the body force per unit volume.

The relation between stress and strain is given by the generalized Hooke's law:

$$\sigma_{ij} = 2\mu\epsilon_{ij} + \lambda\epsilon_{kk}\delta_{ij}, \quad (2.2)$$

where  $\mu$  and  $\lambda$  are the *Lamé constants*,  $\epsilon_{ij}$  is the strain tensor and  $\delta_{ij}$  is the *Kronecker delta*. Lamé constants are related to Young Modulus and Poisson ratio:

$$E = \frac{\mu(2\mu + 3\lambda)}{\lambda + \mu} \quad (2.3)$$

$$\nu = \frac{\lambda}{2(\lambda + \mu)} \quad (2.4)$$

Substituting Eq. (2.2) into Eq. (2.1), we obtain:

$$\rho \frac{\partial^2 u_i}{\partial t^2} = \frac{\partial}{\partial x_j} (2\mu\epsilon_{ij} + \lambda\epsilon_{kk}\delta_{ij}). \quad (2.5)$$

Relation between strain and displacement is given by:

$$\epsilon_{ij} = \frac{1}{2} \left( \frac{\partial u_i}{\partial x_j} + \frac{\partial u_j}{\partial x_i} \right). \quad (2.6)$$

Substituting Eq. (2.6) into Eq. (2.5), and expressing the result in vector notation, we obtain the Navier equations of linear elasticity:

$$\rho \frac{\partial^2 \mathbf{u}}{\partial t^2} = \mu \nabla^2 \mathbf{u} + (\mu + \lambda) \nabla (\nabla \cdot \mathbf{u}) + \mathbf{f}, \quad (2.7)$$

where  $\mathbf{u}$  is the displacement vector and  $\mathbf{f}$  is the body force vector.

### 2.3 Electrostatics: Piezoelectric effect

A piezoelectric material is capable of converting electrical energy into mechanical energy and vice versa. The direct piezoelectric effect states that these materials, when subjected to mechanical stress, generate a proportional electric charge. Gas lighters, and some acceleration and pressure sensors make use of the direct piezoelectric effect. The inverse piezoelectric effect indicates that the same materials, when subjected to an electrical field, become proportionally strained. Buzzers and force sensors use the inverse piezoelectric effect. The linear piezoelectric constitutive strain-charge relations for isothermal conditions using contracted matrix notation are:

$$S_{ij} = s_{jk}^E T_k + d_{kj} E_k \quad (2.8)$$

$$D_i = d_{ij} T_j + \epsilon_{ij}^T E_j \quad (2.9)$$

where  $S$  is the mechanical strain,  $s^E$  is the elastic compliance coefficient at constant electric field,  $T$  is the mechanical stress,  $d$  is the piezoelectric strain coefficient,  $E$  is the electric field,  $D$  is the electric displacement and  $\epsilon^T$  is the permittivity at constant stress.

Piezoelectric strain coefficient matrix for PZT-5H is as follows:

$$[d_{ij}] = \begin{bmatrix} 0 & 0 & d_{31} \\ 0 & 0 & d_{31} \\ 0 & 0 & d_{33} \\ 0 & d_{15} & 0 \\ d_{15} & 0 & 0 \\ 0 & 0 & 0 \end{bmatrix} \quad \begin{aligned} d_{31} &= -274 \times 10^{-12} \text{ CN}^{-1} \\ d_{33} &= 593 \times 10^{-12} \text{ CN}^{-1} \\ d_{15} &= 741 \times 10^{-12} \text{ CN}^{-1} \end{aligned}$$

If there is no residual stress, the first term of right side part of (2.8) is equal to zero, also for a thin circular membrane it can be assumed that the strain is produced only in the radial direction. The simplified relation becomes:

$$S_1 = d_{31} E_3$$

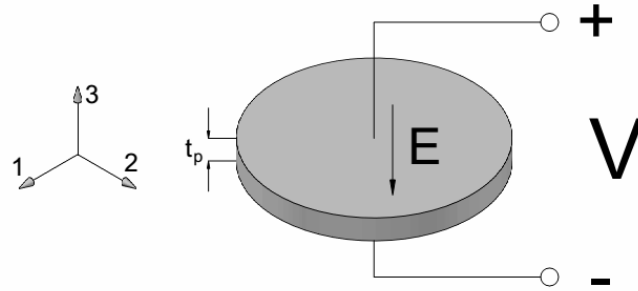


Fig. 2.3.: Schematic of the actuation system

In this case, as showed in Figure 2.3:

$$E_3 = \frac{V}{t_p}$$

the final relation is as follows:

$$S_1 = d_{31} \frac{V}{t_p} \quad (2.10)$$

## 2.4 Fluid dynamics: Poiseuille flow

In the *continuum hypothesis* it is assumed that a fluid property have a definite value at every point in space. This is valid since the characteristic length scale is large when compared with the mean intermolecular distance of the fluid. The characteristic length of the system under analysis in this work is much bigger than the intermolecular distance of water, for that reason, the *continuum* is going to be used. The following assumptions are used for fluid dynamics analysis:

1. The fluid flow is isothermal and laminar.
2. Water is in liquid phase in all cases, and it is considered incompressible, inviscid and Newtonian.
3. There is no more than 1% of air in the analyzed volume of water.

### 2.4.1 Navier-Stokes equations

Because of assumption 1, conservation of thermal energy is not part of the analysis and conservation of mass and momentum can fully describe fluid motion.

The Navier-Stokes continuity equation –conservation of mass– in differential general form is [2]:

$$\frac{\partial \rho}{\partial t} + \nabla \cdot (\rho \mathbf{u}) = 0, \quad (2.11)$$

where  $\mathbf{u}$  is the fluid velocity vector and  $\rho$  is the density of the fluid.

For incompressible flow, Eq. (2.11) reduces to:

$$\nabla \cdot \mathbf{u} = 0. \quad (2.12)$$

The conservation of momentum is described through the Navier-Stokes equation of motion, which in differential general form is [3]:

$$\rho \frac{\partial \mathbf{u}}{\partial t} + \rho (\mathbf{u} \cdot \nabla) \mathbf{u} + \nabla p - \mu \nabla^2 \mathbf{u} - (\lambda + \mu) \nabla (\nabla \cdot \mathbf{u}) = \mathbf{f}, \quad (2.13)$$

where  $p$  is the pressure,  $\mu$  is the dynamic viscosity,  $\lambda$  is a second viscosity coefficient and  $\mathbf{f}$  is the body force vector.

For incompressible flow, Eq. (2.13) becomes:

$$\frac{\partial \mathbf{u}}{\partial t} + (\mathbf{u} \cdot \nabla) \mathbf{u} = -\frac{1}{\rho} \nabla p + \nu \nabla^2 \mathbf{u}, \quad (2.14)$$

where  $\nu$  is the kinematic viscosity.

### 2.4.2 Continuity equation

For the purposes of this work it is necessary to derive a simpler solution of the continuity equation. The *divergence theorem* is:

$$\iiint_V (\nabla \cdot \mathbf{u}) dV = \iint_S (\mathbf{u} \cdot \mathbf{n}) dS. \quad (2.15)$$

Substituting Eq. (2.12) into Eq. (2.15):

$$\oiint_S (\mathbf{u} \cdot \mathbf{n}) dS = 0 \quad (2.16)$$

Having a streamtube like the one showed in Fig. 2.4, it is possible to decompose Eq. (2.16) into:

$$-\iint_{A_1} v_1 dS + \iint_{A_2} v_2 dS = 0, \quad (2.17)$$

simplifying and deriving we have:

$$v_1 A_1 = v_2 A_2 \quad (2.18)$$

$$Q_1 = Q_2, \quad (2.19)$$

which is the simpler form for continuity equation in an incompressible flow with no flow sources.

### 2.4.3 Hagen–Poiseuille equation

An exact solution of the Navier-Stokes equations can be obtained for the flow in a pipe driven by a constant pressure gradient. Consider a cylinder with uniform cross-section of radius  $R$  with an axis coincident with the  $x$  direction, as showed in Fig. 2.5. Assuming the pressure gradient and the velocity act also in the  $x$  direction and substituting the velocity vector  $\mathbf{u} = (u_1(r), 0, 0)$  in Eq. (2.14) one can obtain –for steady state–:

$$-\frac{1}{\rho} \nabla p = \frac{\nu}{r} \frac{\partial}{\partial r} \left( r \frac{\partial u_1}{\partial r} \right), \quad (2.20)$$

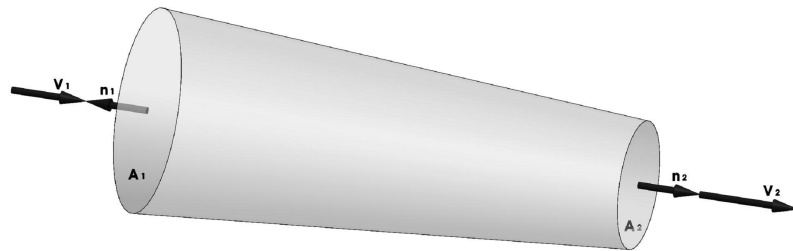


Fig. 2.4.: Arbitrary flow streamtube

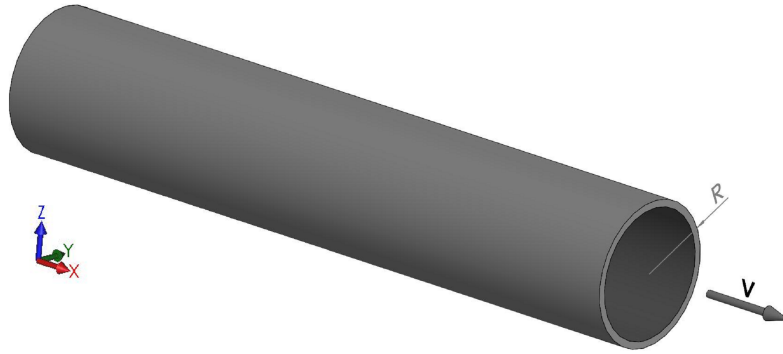


Fig. 2.5.: Poiseuille flow in a pipe

where  $r$  is the radial position inside the pipe.

Since the pressure gradient only changes with  $x$  it can be substituted for  $-\nabla p = -\partial p/\partial x$ . Integrating two times with respect to  $r$  and determining the constants of integration assuming no slip boundary condition in  $r = R$ , the following is obtained:

$$u_1(r) = -\frac{\partial p}{\partial x} \frac{1}{4\mu} (R^2 - r^2). \quad (2.21)$$

Assuming that the pressure decreases linearly in the direction of the flow, then  $-\partial p/\partial x = (p_1 - p_2)/L = p_{12}/L$ , so Eq. (2.21) becomes:

$$u_1(r) = \frac{p_{12}}{L} \frac{1}{4\mu} (R^2 - r^2), \quad (2.22)$$

where  $L$  is the length of the pipe and  $p_{12}$  is the pressure difference the two ends of the pipe.

The flow rate  $Q$  can be obtained integrating the velocity vector over the cross section of the pipe:

$$Q = \iint_S \mathbf{u} \cdot \mathbf{nd}S = \int_0^{2\pi} \int_0^R u_1(r) r dr d\theta. \quad (2.23)$$

Substituting Eq. (2.22) into Eq. (2.23) and solving the double integral yields to:

$$Q = \frac{p_{12}}{L} \frac{\pi R^4}{8\mu}, \quad (2.24)$$

Substituting  $Q = v \cdot A$  into Eq. (2.24), where  $v$  is the average velocity and  $A$  the cross sectional area of the pipe, one finds that:

$$v = \frac{p_{12}}{L} \frac{D^2}{32\mu}, \quad (2.25)$$

where  $D = 2 \cdot R$  is the diameter of the pipe.

It is necessary to consider the Reynolds number to verify the validity of the laminar flow assumption. Knowing that:

$$Re = \frac{v\rho D}{\mu}. \quad (2.26)$$

For any non-circular cross sectional area, the *hydraulic diameter*  $D_H$ , has to be used instead of the radius of the tube as follows:

$$D_H = \frac{4 \cdot A}{W_P}, \quad (2.27)$$

where  $W_P$  is the wetted perimeter.

However, in extremely narrow shapes –our case– the hydraulic diameter is equal to two times the smallest dimension of the channel [4]. That is:

$$D_H = 2b \quad (2.28)$$

where  $b$  is the height of the channel, supposing the width is at least ten times bigger than height.

#### 2.4.4 Pressure loss in Poiseuille flow

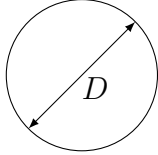
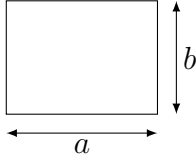
Darcy's formula for pressure loss in pipes states that [4]:

$$p_{12} = f_D \frac{L}{D} \frac{\rho v^2}{2}, \quad (2.29)$$

where  $f_D$  is the Darcy friction factor. For laminar flow this factor can be approximated as:

$$f_D = \frac{k_g}{Re}, \quad (2.30)$$

Table 2.1.: Values of  $k_g$  for different geometries [5].

Tube geometry		$k_g$
Circle		
	-	64
Rectangle	$a/b$	
	1	56.92
	2	62.20
	3	68.38
	4	72.92
	6	78.80
	8	82.32
	$\infty$	96.00

where  $k_g$  is a geometry factor given by Table 2.1.

Substituting Eq. (2.26) and Eq. (2.30) into Eq. (2.29), we obtain:

$$p_{12} = \frac{\mu k_g L v}{2D^2}, \quad (2.31)$$

for the special case of a circular pipe we can substitute  $k_g = 64$ , that yields to:

$$p_{12} = \frac{32\mu L v}{D^2}, \quad (2.32)$$

which is, as expected, the same result obtained in Eq.(2.25). This just illustrate the validity of the Hagen-Poiseuille law under laminar flow conditions in a circular pipe.

However, for a pipe of rectangular cross section we have:

$$p_{12} = \frac{\mu k_g L v}{2D_H^2}, \quad (2.33)$$

in a narrow channel,  $D_H = 2b$  and the geometry factor becomes  $k_g = 96$ , substituting this in Eq. (2.33) we obtain:

$$p_{12} = \frac{12\mu Lv}{b^2}, \quad (2.34)$$

knowing that  $A = ab$ , the same expression in terms of  $Q$  will be:

$$p_{12} = \frac{12\mu LQ}{Ab^2} = \frac{12\mu LQ}{ab^3}, \quad (2.35)$$

This expression is valid for a narrow channel, however, Bruus in [6] derived an analytical solution for Poiseuille flow in a pipe or channel of rectangular cross section, that is:

$$p_{12} = \frac{12\mu LQ}{ab^3} \left[ 1 - 0.63 \frac{b}{a} \right]^{-1} \quad (2.36)$$

There exists another form of expressing the Darcy's formula, specially developed for minor losses on fittings and accessories:

$$p_{12} = K_x \frac{\rho v^2}{2}, \quad (2.37)$$

where  $K_x$  is the resistance coefficient. If we compare this expression with Eq. (2.29), it is clear that:

$$K_x = f_D \frac{L}{D}, \quad (2.38)$$

in this context  $L$  is known as the equivalent length  $L_e$ , and it is defined as the length of straight and circular pipe of diameter  $D$  that will cause the same pressure drop as the obstruction under the same flow conditions [4].

If a value of  $K_x$  is known, it can be converted into an equivalent length using:

$$L_e = \frac{K_x D}{f_D}. \quad (2.39)$$

## 2.5 Dynamic system modeling: Equivalent electric circuits

Real world dynamic systems are very different in nature but their behavior is well described by the same law, the conservation of energy. The different disciplines

of physics, such as mechanical, electrical, hydraulic and others, developed their own models to describe the systems of their interest [7].

Nowadays, in state-of-the-art developments, it is difficult to find a system that could be well described as an isolated one. Links between different physics become more and more important as systems become smaller and more interrelated to each other. However, multidisciplinary treatment of dynamics systems in scientific literature is still scarce [8].

In this context, a generalized model applicable for all of these disciplines is highly desirable. Through the years, there have been efforts to achieve that. Some examples are:

- *Bond graphs*: proposed by Henry Paynter in 1959 [9], is a modeling method based on power flow diagrams which is independent of physical domain [7].
- *Generalized Network*: proposed by Alfaro in 1986 [10], is also based on power flow, but the graphic representation and laws are taken from the electrical networks.

There are also electrical-mechanical analogies like Ogata's *force-voltage* and *force-current* [11] which are equivalent to Nise's *series analog* and *parallel analog* [12].

The approach of this work is based in the *Equivalent Circuit Theory*, a set of electrical analogies with other systems that has been built through the years by the scientific community, some of the analogies are covered in the *Generalized Network*, but not all of them.

In order to understand the basis of this modeling technique, first we have to introduce the two kinds of variables, the *transvariable* –also known as *across variable*– and the *pervariable* –or *through variable*–. A transvariable need two different points of the system to be measured, by contrast a pervariable needs only one point [8]. Both transvariables and pervariables can be classified as *rate* or *state* variables. For example, in fluid mechanics both flow rate and volume are pervariables, but flow rate is a *rate* variable and volume is a *state* variable. In this case, as in the general case,

Table 2.2.: Transvariables and pervariables of dynamic systems [8].

System	Rate Pervariable ( $f$ )	State Pervariable ( $h$ )	Rate Transvariable ( $v$ )	State Transvariable ( $\chi$ )
Mechanical Translational	Force ( $F$ )	Momentum ( $\mathcal{P}$ )	Velocity Difference ( $v$ )	Displacement ( $x$ )
Mechanical Rotational	Torque ( $\tau$ )	Angular Momentum ( $h$ )	Angular Velocity Difference ( $\omega$ )	Angular Displacement ( $\theta$ )
Electrical	Current ( $I$ )	Charge ( $q$ )	Electric Potential Difference ( $V$ )	Flux linkage ( $L$ )
Fluidic	Flow Rate ( $Q$ )	Volume ( $\mathcal{V}$ )	Pressure Difference ( $p$ )	Momentum of Pressure ( $\Gamma$ )
Thermal	Heat Flux ( $q$ )	Heat ( $H$ )	Temperature Difference ( $T$ )	-

the *rate* variable is the time derivative of the *state* variable. Analogies for different systems are summarized in Table 2.2.

The concept of *energy port* is used as the place in the element where the power exchange is done, this term is equivalent to *port* in *Bond Graphs*. A representation is shown on Figure 2.6.

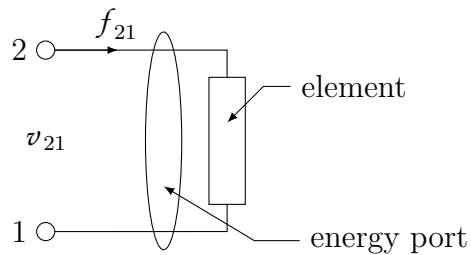


Fig. 2.6.: Schematic of an energy port [13]

There are four types of variables, the *rate transvariable* ( $v$ ), the *state transvariable* ( $h$ ), the *rate pervariable* ( $f$ ) and the *state pervariable* ( $\chi$ ). Their relations are the following:

$$v_{21} = \mathcal{Z}_g f_{21} \quad (2.40)$$

$$v_{21} = \mathcal{D} \chi_{21} \quad (2.41)$$

$$f_{21} = \mathcal{D} h_{21}, \quad (2.42)$$

where  $\mathcal{Z}_g$  is the generalized impedance operator and  $\mathcal{D}$  is the differential operator.

The three different possibilities for generalized impedances are summarized in Table 2.3.

Table 2.3.: Constitutive relation and generalized impedance of the basic elements.

Generalized element	Constitutive relation	Generalized impedance
Resistance	$v_{21} = \mathcal{R}_g f_{21}$	$\mathcal{Z}_{\mathcal{R}} = \mathcal{R}_g$
Capacitance	$\mathcal{C}_g \mathcal{D} v_{21} = f_{21}$	$\mathcal{Z}_{\mathcal{C}} = 1/\mathcal{D} \mathcal{C}_g$
Inductance	$\mathcal{L}_g \mathcal{D} f_{21} = v_{21}$	$\mathcal{Z}_{\mathcal{L}} = \mathcal{D} \mathcal{L}_g$

Most of the common elements of the electric networks can be easily related to their analogous counterparts using the above definitions.

### 2.5.1 Electrical Equivalent Networks for Fluid Dynamics Modeling

As showed in Table 2.2, in fluidic systems, volume is the state pervariable  $h = \mathcal{V}$ , volumetric flow rate is the rate pervariable,  $f = Q$ , and the pressure difference is the rate transvariable,  $v = p$ . The commonly used constitutive relations are based on Eq. (2.40) and (2.42) as:

$$p_{12} = \mathcal{Z}_g Q \quad (2.43)$$

$$Q = \mathcal{D} \mathcal{V} \quad (2.44)$$

## Hydraulic Resistance

This element offers resistance to the flow, it will produce a pressure drop due to the power dissipation (viscous dissipation), some examples are: filters, restrictions or expansions, turbulent flow, capillary action, and others, and are defined as:

$$\mathcal{Z}_{\mathcal{R}} = \mathcal{R}_{hyd} = \frac{p_{12}}{Q} \quad (2.45)$$

the resistance to flow of any obstruction of a given equivalent length of rectangular pipe  $L_e$  is:

$$\mathcal{R}_{hyd} = \frac{12\mu L_e}{ab^3} \left[ 1 - 0.63 \frac{b}{a} \right]^{-1} \quad (2.46)$$

## Hydraulic Capacitance: Compliance

An element which store energy as a function of pressure is an hydraulic capacitor. Compliance exists because fluid and solids are not rigid in all cases, examples of hydraulic capacitors are: a membrane or elastic tube and a bubble of compressible fluid. Compliance is defined as:

$$\mathcal{C}_{hyd} = \frac{Q}{\mathcal{D}p} = \frac{\mathcal{D}\mathcal{V}}{\mathcal{D}p} \quad (2.47)$$

$$\mathcal{Z}_c = \frac{1}{\mathcal{D}\mathcal{C}_{hyd}} \quad (2.48)$$

There are two kinds of compliances related to this work::

1. *Open reservoir*: consider a vertical reservoir of constant cross-sectional area  $A$ , which is originally at a hight  $h_1$  and then is filled until it reaches a height of  $h_2$  in a time  $t$ . The change in pressure and volume will be:

$$\mathcal{D}p_{12} = \frac{\rho g(h_2 - h_1)}{t} \quad (2.49)$$

$$\mathcal{D}\mathcal{V} = Q = \frac{A(h_2 - h_1)}{t}, \quad (2.50)$$

which means that the compliance of an open reservoir is:

$$\mathcal{C}_{hyd} = \frac{A}{\rho g}. \quad (2.51)$$

2. *Bubble of compressible fluid:* consider a bubble of air which slowly (isothermally) changes its pressure. Since ideal gas law is:

$$p\mathcal{V} = mRT, \quad (2.52)$$

where  $m$  is the mass of gas,  $R$  is the specific gas constant and  $T$  is the temperature. A very small change in pressure will be:

$$\mathcal{D}p = \mathcal{D}m \frac{RT}{\mathcal{V}} = \rho \mathcal{D}\mathcal{V} \frac{RT}{\mathcal{V}} \quad (2.53)$$

which means that the compliance of an air bubble is:

$$\mathcal{C}_{hyd} = \frac{\mathcal{V}}{\rho RT} = \frac{\mathcal{V}}{p_r} \quad (2.54)$$

where  $p_r$  is a reference pressure.

### Hydraulic Inductance: Inertance

The inertance, as its name indicates, is related to the inertial forces required to accelerate a fluid in a pipe. It is defined as:

$$\mathcal{L}_{hyd} = \frac{p_{12}}{\mathcal{D}Q} \quad (2.55)$$

$$\mathcal{Z}_{\mathcal{L}} = \mathcal{D}\mathcal{L}_{hyd}. \quad (2.56)$$

Consider an horizontal pipe of length  $L$  and constant cross-section area  $A$ , which has an incompressible fluid of density  $\rho$  enclosed in a volume  $\mathcal{V} = AL$ . Assuming that the only force acting on the system is a pressure difference  $p_{12}$  we can write Newton second law as:

$$p_{12}A = \rho LA \mathcal{D}v, \quad (2.57)$$

and since  $Q = vA$ , we have:

$$p_{12}A = \rho L \mathcal{D}Q, \quad (2.58)$$

this means we know that the inertance of a volume of fluid flowing inside a pipe is:

$$\mathcal{L}_{hyd} = \frac{\rho L}{A}. \quad (2.59)$$

### 3. PIEZOELECTRIC VALVELESS MICROPUMP EQUIVALENT CIRCUIT MODEL

The geometry of the micropump is overviewed in Section 3.1. A general explanation of the system and its lumped elements is done in Section 3.2, determination of the parameters of these elements is covered in Section 3.3. At the end of the chapter, in Section 3.5, the developed model is shown.

#### 3.1 Geometry of the micropump

Since most of the characteristics of the lumped elements are related to the geometry of the micropump, an overview is necessary. A deeper presentation of the fabrication method and its relation with the geometry is done in Section 4.2.

The pump consist of a circular chamber –where the actuation take place– connected to two diffuser/nozzle structures, which at the same time, are the inlet and outlet, left and right respectively in Fig. 3.1. These two ports are connected to a pair of calibrated pipettes which act as reservoirs.

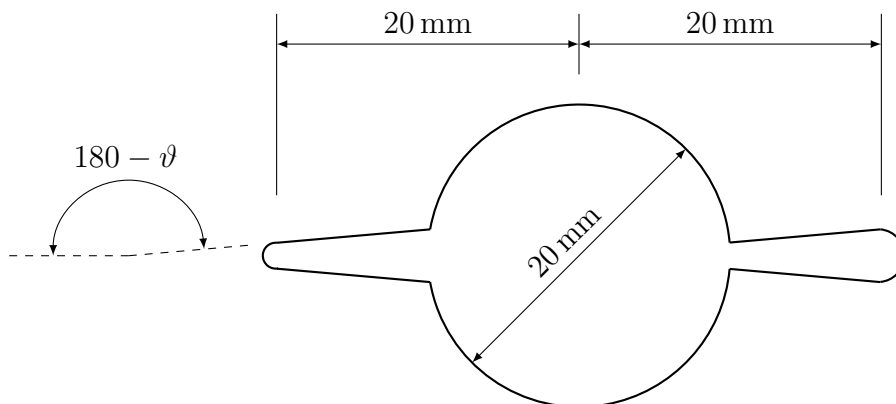


Fig. 3.1.: Geometry of the micropump.

Table 3.1.: Input parameters of lumped elements.

Element	Parameter	Description	Value
Actuator	$D_{pz}$	Piezo disc diameter	16 mm
	$t_{pz}$	Piezo disc thickness	160 $\mu\text{m}$
	$D_{br}$	Brass electrode diameter	20 mm
	$t_{br}$	Brass electrode thickness	200 $\mu\text{m}$
	$t_{gs}$	Glass membrane thickness	150 $\mu\text{m}$
	$p_{gs}$	Pressure under glass membrane*	1470 Pa
	$V_p$	Peak voltage	169.7 V
	$f$	Frequency	60 Hz
	$\omega$	Angular frequency	376.99 rad/s
	$T$	Period	16.67 ms
Chamber	$D_{ch}$	Chamber diameter	20 mm
	$t_{ch}$	Chamber depth	205 $\mu\text{m}$
	$\mathcal{V}_{ch}$	Nominal volume	64.4026 mm <sup>3</sup>
	$\mathcal{V}_{bub}$	Bubble volume (1% of $\mathcal{V}_{ch}$ )	$6.4403 \times 10^{-10}$ m <sup>3</sup>
	$p_r$	Reference pressure ( $p_0 + p_{gs}$ )	102 470 Pa
Inlet and outlet water columns	$D_{pip}$	Internal diameter of pipette top	2.95 mm
	$D_{pid}$	Internal diameter of the pipette bottom	1.60 mm
	$D_{ned}$	Internal diameter of the neddle	0.605 mm
	$A_{pip}$	Cross-section of pipette	$6.8349 \times 10^{-6}$ m <sup>2</sup>
Inlet and outlet	$\vartheta$	Angle of nozzle/diffuser	2.5°
	$L_{nd}$	Nominal length of nozzle/diffuser	4 mm

\*Assumed to be a constant value of 15mm of water.

### 3.2 Overview of the system

The equivalent circuit model of the piezoelectric micropump consist of six subsystems, as shown in Fig. 3.2, which are:

- *Actuator*: it consist of an independent sinusoidal voltage source and a voltage controlled current –flow– source grounded on  $p_0$  and controlled by the terminal

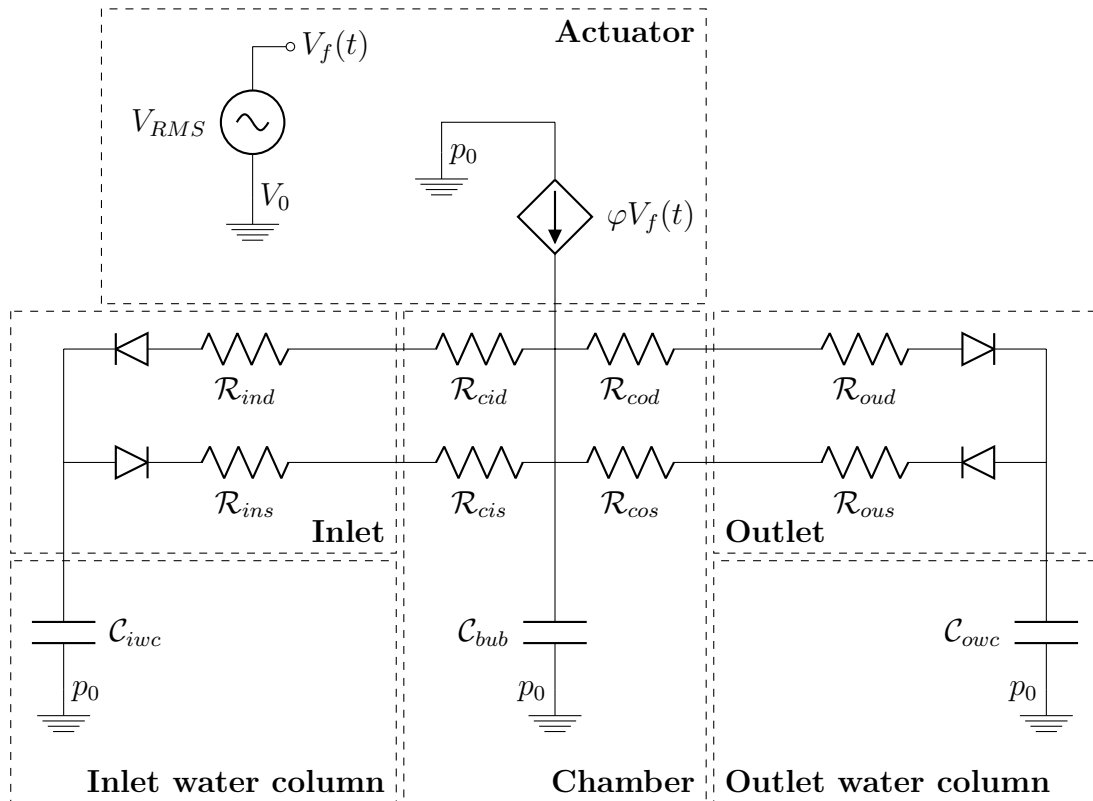


Fig. 3.2.: Equivalent circuit model.

$V_f(t)$ , with a gain  $\varphi$ . The parameters of the current source are calculated solving the membrane deflection as a function of the applied voltage to the piezoelectric actuator and then determining the associated change of volume as a function of time.

- *Chamber*: is where the actuator operates, the volume of the chamber is constantly changing during the actuation process, producing a volume suction or discharge as a function of the membrane deflection.
- *Inlet and outlet*: there are two combinations of a diode in series with an hydraulic resistance for each port, which are used to model the behavior of these ports under opposite directions of flow in terms of pressure loss.

- *Inlet and outlet water columns:* as part of the experimental setup, two calibrated pipettes are connected to both the inlet and outlet, these water columns are modeled as capacitors with an initial voltage, which represent the initial height of the fluid in the pipettes.

### 3.3 Determination of output parameters of lumped elements

Using the input parameters summarized in Table. 3.1, a derivation of the output parameters of the lumped elements will be done using the relations obtained in Section 2.5.

#### 3.3.1 Piezoelectric actuator model

The actuator model will be fully described by determining the gain  $\varphi$ . This gain is the relation between the value of the voltage supplied by the source and the flow rate provided by the dependent current –flow– source. The use of gain alone, without including the phase shift is because the interest of this work is in the stable state operation.

Considering that the actuator is circular, we can use its axial symmetry to simplify the model. Using this simplification a *2D axisymmetric* simulation was set in COMSOL Multiphysics <sup>®</sup>.

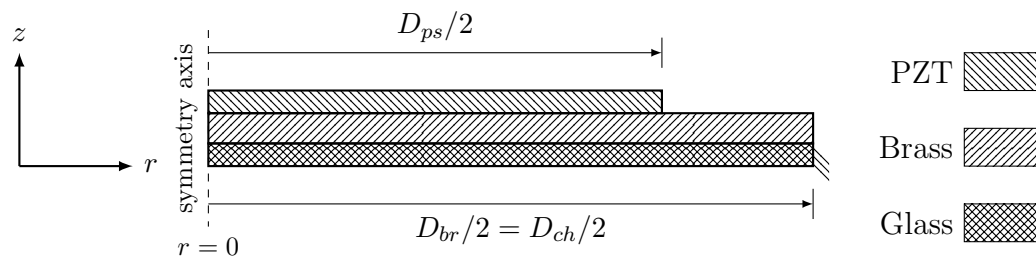


Fig. 3.3.: Axisymmetric geometry of actuator.

In order to obtain the flow rate displaced by the actuator, the following steps were carried out –detailed information in Table 3.2–:

1. Geometry and materials were defined as shown in Fig. 3.3. None of the adhesive materials, neither the top electrode film, were included in the analysis.
2. *Solid mechanics* and *electrostatics physics interfaces* were coupled using the *piezoelectric effect*.
3. A sinusoidal waveform  $V_f(t)$ , was defined with frequency  $f$ , and amplitude  $V_p$ . Its output is applied as the *electric potential* of the top electrode of PZT actuator. Bottom electrode is defined as *ground*.
4. A pressure  $p_{gs}$  is applied in positive  $z$  direction onto the downside boundary of the glass membrane.
5. The variable  $A_w(t)$  was defined by means of an *integration operator* applied in the downside boundary of the glass, to integrate the deflection  $w_{gs}(r, t)$  of the membrane over its radius, that is:

$$A_w(t) = \int_0^{D_{ch}/2} w_{gs}(r, t) dr. \quad (3.1)$$

6. The variable  $\bar{r}(t)$ , the centroid of  $A_w(t)$ , was defined as:

$$\bar{r}(t) = \frac{S_z(t)}{A_w(t)}, \quad (3.2)$$

where  $S_z(t)$  is the first moment of  $A_w(t)$ , defined as:

$$S_z(t) = \int_0^{D_{ch}/2} r w_{gs}(r, t) dr. \quad (3.3)$$

7. The variable  $\mathcal{V}_f(t)$ , the displaced volume, was defined using Pappus–Guldinus theorem, that is:

$$\mathcal{V}_f(t) = A_w(t) \cdot 2\pi\bar{r}(t) \quad (3.4)$$

8. The variable  $Q_f(t)$ , the flow rate displaced by the actuator, was defined as the derivative of the displaced volume over time, as follows:

$$Q_f(t) = \frac{dV_f(t)}{dt}. \quad (3.5)$$

9. A time-dependent study is solved from 0 to  $5T$  seconds with time step of  $T/100$  seconds, input  $u(t) = V_f(t)$  and output  $y(t) = Q_f(t)$  are plotted, as shown in Fig. 3.4.

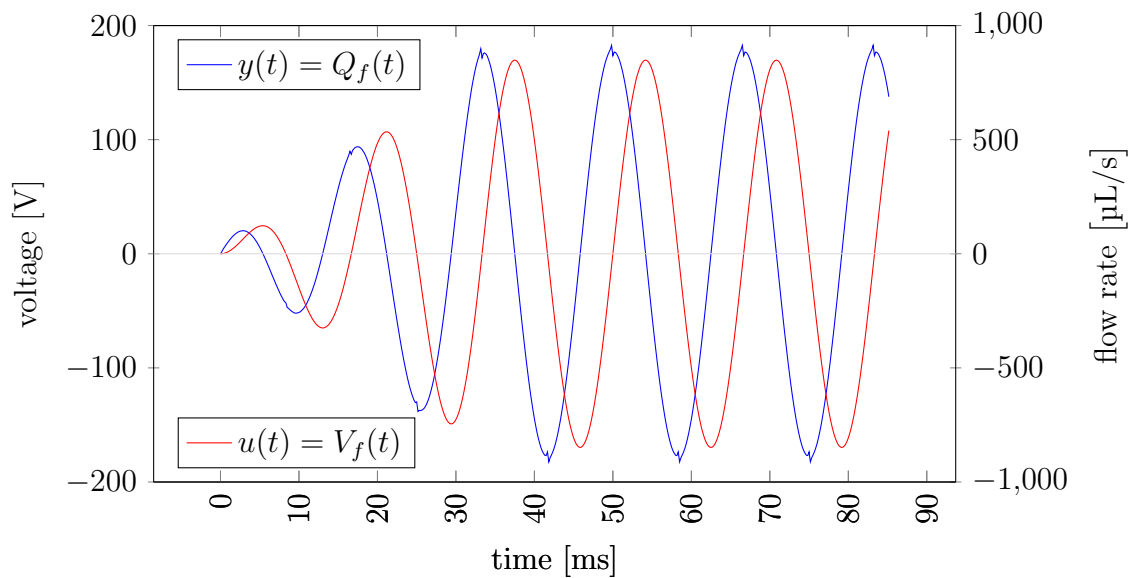


Fig. 3.4.: Waveforms of input  $u(t)$ , and output  $y(t)$ , obtained from the simulation

Once results are obtained, it is found that the output function  $y(t)$ , is a sinusoidal wave with amplitude  $Q_p = 8.9372 \times 10^{-7} \text{ m}^3/\text{s}$ , and phase shift of  $\phi \approx 90^\circ$ , relative to the input function  $u(t)$  –determined using MATLAB® curve fitting tools–. This means that this system is an LTI –Linear time-invariant system–, which implies that its amplification factor and phase shift are as shown in Eqs. (3.9). These two functions are defined, and their Laplace transforms are shown in Eqs. (3.6).

Table 3.2.: Simulation configurations for actuator.

<b>Parameters</b>			
<i>COMSOL name</i>	<i>Document symbol</i>	<i>COMSOL name</i>	<i>Document symbol</i>
ch.d	$D_{ch}$	gs.t	$t_{gs}$
pz.d	$D_{pz}$	pz.t	$t_{pz}$
br.d	$D_{br}$	br.t	$t_{br}$
f	$f$	omega	$\omega$
Vp	$V_p$	Pe	T
press	$p_{gs}$		
<b>Ramp</b>			
<i>Name</i>	<i>Location</i>	<i>Slope</i>	<i>Cutoff</i>
rm1	0	f/2	1
<i>Smoothing</i>	<i>Transition zone</i>		
at cutoff	1/(4f)		
<b>Waveform</b>			
<i>Name</i>	<i>Type</i>	<i>Ang. freq.</i>	<i>Phase</i>
wv1	sine	omega	0
<i>Amplitude</i>			
Vp			
<b>Integration coupling</b>			
<i>COMSOL Name</i>	<i>Entity level</i>	<i>Applied in</i>	
intop1	boundary	downside boundary of glass	
<b>Variables</b>			
<i>COMSOL Name</i>	<i>Document symbol</i>	<i>COMSOL definition</i>	
Vpz	$V_f(t)$ (ramped)	rm1(t[1/s])*wv1(t[1/s])	
pressvar	$p_{gs}$ (ramped)	rm1(t[1/s])*press	
area	$A_w(t)$	comp1.intop1(comp1.w)	
cent	$\bar{r}(t)$	comp1.intop1(r*comp1.w)/area	
flow	$Q_f(t)$	d(area,TIME)*(2*pi*cent)	

$$u(t) = V_p \sin(\omega t) \quad \mathcal{L}\{u(t)\} = U(s) = V_p \frac{\omega}{s^2 + \omega^2} \quad (3.6a)$$

$$y(t) = Q_p \sin(\omega t + \phi) \quad \mathcal{L}\{y(t)\} = Y(s) = Q_p \frac{s \sin(\phi) + \omega \cos(\phi)}{s^2 + \omega^2} \quad (3.6b)$$

The transfer function of a system is defined as:

$$H(s) = \frac{Y(s)}{U(s)}, \quad (3.7)$$

considering that  $\phi \approx 90^\circ$ , we have:

$$H(s) = \omega \frac{Q_p}{V_p} \frac{1}{s}, \quad H(j\omega) = \frac{Q_p}{V_p} \frac{1}{j}, \quad (3.8)$$

for LTI systems we have:

$$\text{Amplification factor} \Rightarrow |H(j\omega)|. \quad (3.9a)$$

$$\text{Phase shift} \Rightarrow \angle H(j\omega). \quad (3.9b)$$

In this work we are only interested in the amplification factor, which is:

$$|H(j\omega)| = \left| \frac{Q_p}{V_p} \frac{1}{j} \right| = \frac{Q_p}{V_p} = \varphi \quad (3.10)$$

Substituting numerical values for  $Q_p$  and  $V_p$ , we have:

$$\varphi = 5.2664 \times 10^{-9} \text{ m}^3/\text{Vs} \quad (3.11)$$

### 3.3.2 Chamber

The compliance of an air bubble is modeled using a volume of 1% of the total volume of the chamber –based on qualitative observations carried out during the experiments–, following Eq. (2.54), we have:

$$\mathcal{C}_{bub} = \frac{\mathcal{V}_{bub}}{p_r} \quad (3.12)$$

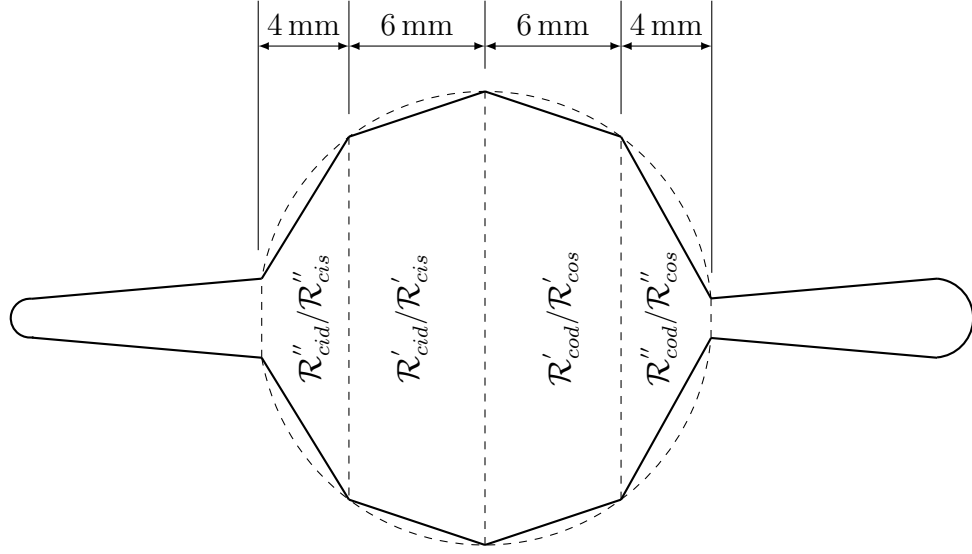


Fig. 3.5.: Geometrical approximation of the chamber.

where  $\mathcal{V}_{bub}$  is the volume of the bubble and  $p_r$  is a reference pressure, representing the average pressure of the bubble. Substituting numerical values from Table. 3.1, we have:

$$\mathcal{C}_{bub} = 2.2626 \times 10^{-15} \text{ m}^3 \text{ Pa}^{-1} \quad (3.13)$$

In order to calculate the hydraulic resistances of the inlet and outlet side of the chamber, a geometrical approximation was used as shown in Fig. 3.5. Using this geometric configurations, a series of simulations were set in COMSOL Multiphysics® as detailed below –more information is shown in Table 3.4.–:

1. Geometry was defined as shown in Fig. 3.5. Values are shown in Table 3.3.
2. *Laminar flow physics interface* was set using the large area as inlet in case of diffuser, or the small area -as inlet- in case of nozzle.
3. The variable  $\mathcal{R}_{hyd}$  is defined as:

$$\mathcal{R}_{hyd} = \frac{p_{12}}{Q} \quad (3.14)$$

4. A *stationary* study with a flow rate of  $Q = \alpha Q_p$ , using a *parametric sweep* from  $\alpha = 0.5$  to 1.5. The study was solved and  $\mathcal{R}_{hyd}$  is determined for each value of  $Q$ .

The obtained value for  $\mathcal{R}_{hyd}$  is not a constant, it varies with the flow rate. For each simulation, a linear approximation was made in order to describe the real behavior of the hydraulic resistance, results are summarized in Table 3.5. Using this linear approximation a variable resistance was defined inside the model, using the approach of Fig. 3.6.

Plots of calculated values of *hydraulic resistances* for chamber are shown in Fig. 3.7 ot 3.9.

### 3.4 Inlet and outlet

For calculation of hydraulic resistances of the inlet and outlet ports there are three different considerations:

- Inlet and outlet nozzle/diffuser structures  $-\mathcal{R}'_{ind}, \mathcal{R}'_{ins}, \mathcal{R}'_{ous}$  and  $\mathcal{R}'_{oud-}$ , are modeled in the same manner as the chamber nozzle/diffuser approximations. Simulation steps and configurations of Table 3.4 are applied, geometrical parameters are shown in Table 3.3, results are summarized in Table 3.5, and plots of calculated values of *hydraulic resistances* are shown in Fig. 3.10 to 3.11
- Inlet and outlet connection with needle tip  $-\mathcal{R}''_{ind}, \mathcal{R}''_{ins}, \mathcal{R}''_{ous}$  and  $\mathcal{R}''_{oud-}$  are modeled as sudden expansion/contraction. Simulation steps and configurations of Table 3.4 are applied, geometrical values are shown in Fig. 3.12, results are summarized in Table 3.5.
- Gradual expansion/contraction between pipettes and needle tips. Simulation steps and configurations of Table 3.4 are applied. In all cases the geometry is a sudden transition between  $D_{pid}$  and  $D_{ned}$ . Results are summarized in Table 3.5.

Table 3.3.: Geometric parameters for simulations.

Element	$a_1$ [mm]	$a_2$ [mm]	$L$ [mm]	$\vartheta$ [ $^\circ$ ]
$\mathcal{R}''_{cid}$ (nozzle)	1.7464	16	3.9618	60.9302
$\mathcal{R}''_{cis}$ (diffuser)				
$\mathcal{R}'_{cid}$ (nozzle)	16	20	6	18.4349
$\mathcal{R}'_{cis}$ (diffuser)				
$\mathcal{R}'_{cod}$ (nozzle)				
$\mathcal{R}'_{cos}$ (diffuser)				
$\mathcal{R}''_{cod}$ (nozzle)	0.8724	16	3.9905	62.1848
$\mathcal{R}''_{cos}$ (diffuser)				
$\mathcal{R}'_{ind}$ (nozzle)	0.9121	1.7464	9.5826	2.5
$\mathcal{R}'_{ins}$ (diffuser)				
$\mathcal{R}'_{ous}$ (nozzle)	0.8724	1.6734	9.1736	2.5
$\mathcal{R}'_{oud}$ (diffuser)				

**Notes:**

1. Definitions:  $a_1$ =smaller width,  $a_2$ =larger width,  $L$ =length
2. Height of channel,  $b = t_{ch} = 205 \mu\text{m}$ , for all cases.

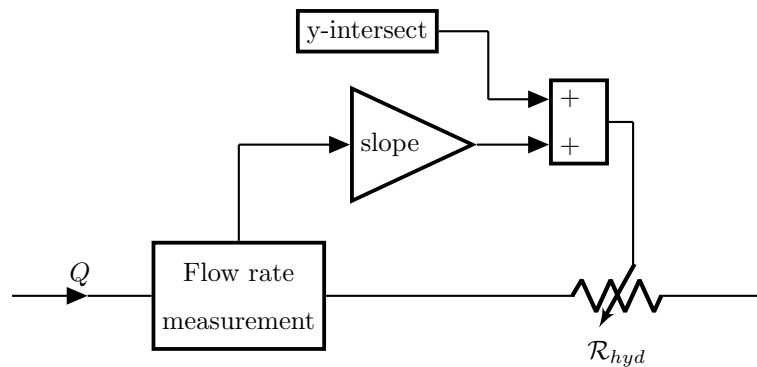


Fig. 3.6.: Variable hydraulic resistance diagram

Table 3.4.: Simulation configurations for nozzles and diffusers.

<b>Parameters</b>			
<i>COMSOL name</i>	<i>Document symbol</i>	<i>COMSOL name</i>	<i>Document symbol</i>
ch.t	$t_{ch}$	Qmax	$Q_p$
Lx	$L$	mult	$\alpha$
LS	$a_1$	LL	$a_2$
<i>COMSOL Name</i>	<i>Document symbol</i>	<i>COMSOL definition</i>	
AS	$A$	ch.t*LS	
AL	$A$	ch.t*LL	
maxv	$v$	Qmax/AS	
<b>Average coupling</b>			
<i>COMSOL Name</i>	<i>Entity level</i>	<i>Applied in</i>	
aveop1	boundary	inlet	
aveop2	boundary	outlet	
<b>Variables</b>			
<i>COMSOL Name</i>	<i>Document symbol</i>	<i>COMSOL definition</i>	
piv	$p_1$	aveop1(p)	
pov	$p_2$	aveop2(p)	
avs	$v$	aveop1(p) for diffuser, aveop2(p) for nozzle	
Q	$Q(t)$	avs*AS	
R	$\mathcal{R}_{hyd}$	(piv-pov)/Q	

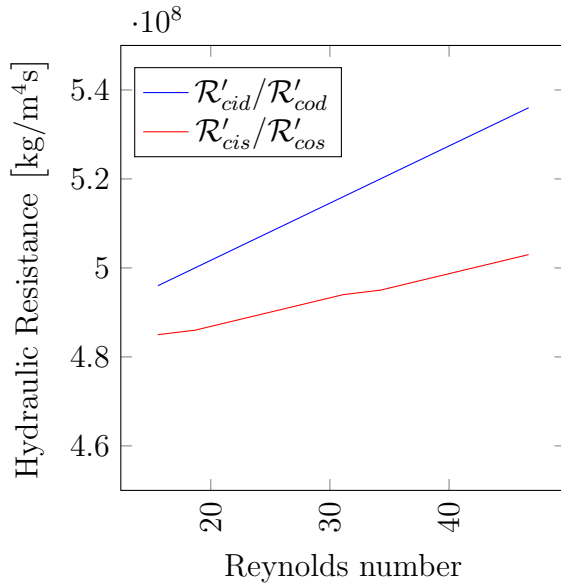


Fig. 3.7.: Curves for  $\mathcal{R}'_{cid}/\mathcal{R}'_{cod}$  and  $\mathcal{R}'_{cis}/\mathcal{R}'_{cos}$  for different values of Reynolds number

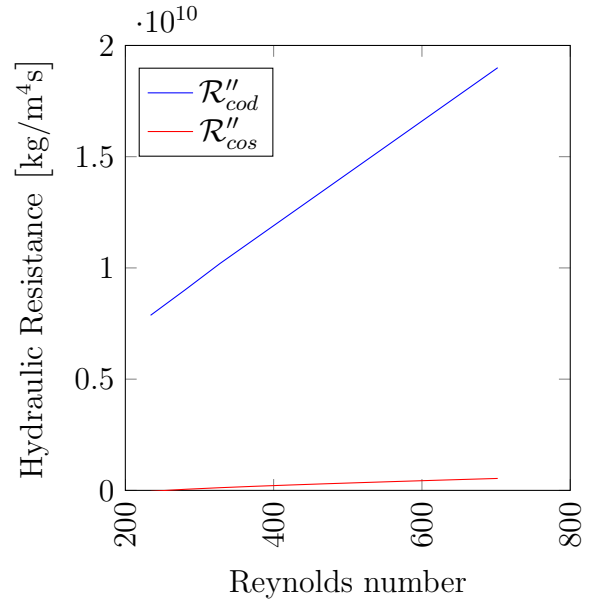


Fig. 3.8.: Curves for  $\mathcal{R}''_{cod}$  and  $\mathcal{R}''_{cos}$  for different values of Reynolds number

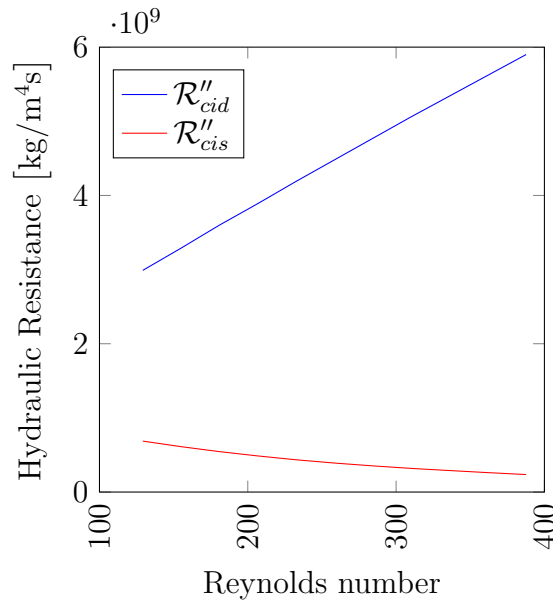


Fig. 3.9.: Values for  $\mathcal{R}''_{cid}$  and  $\mathcal{R}''_{cis}$  for different values of Reynolds number

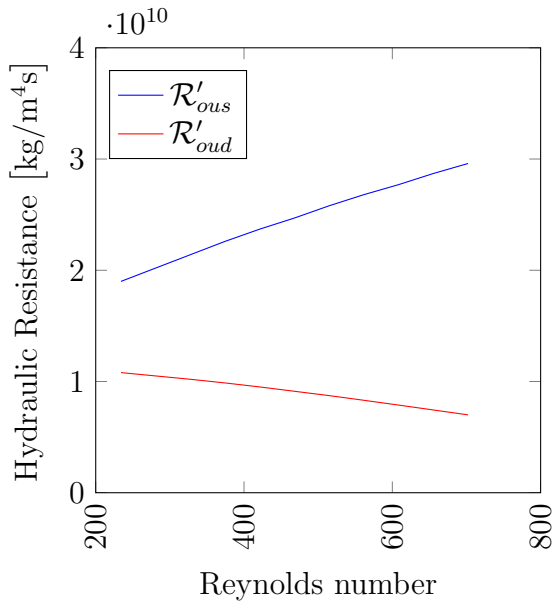


Fig. 3.10.: Curves for  $\mathcal{R}'_{oud}$  and  $\mathcal{R}'_{ous}$  for different values of Reynolds number

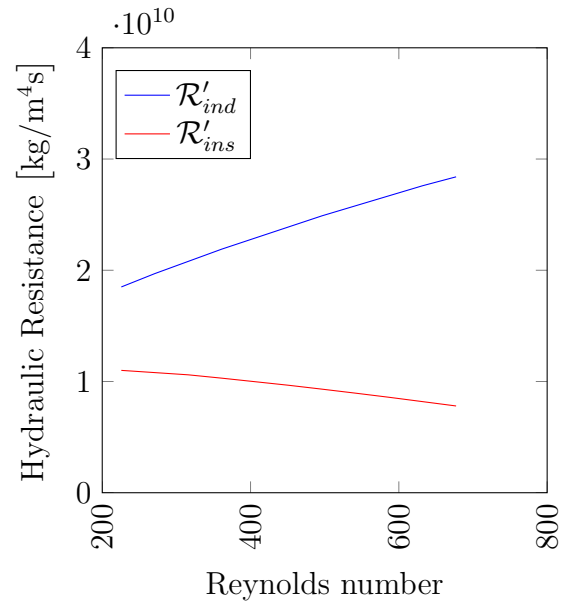


Fig. 3.11.: Curves for  $\mathcal{R}'_{ind}$  and  $\mathcal{R}'_{ins}$  for different values of Reynolds number

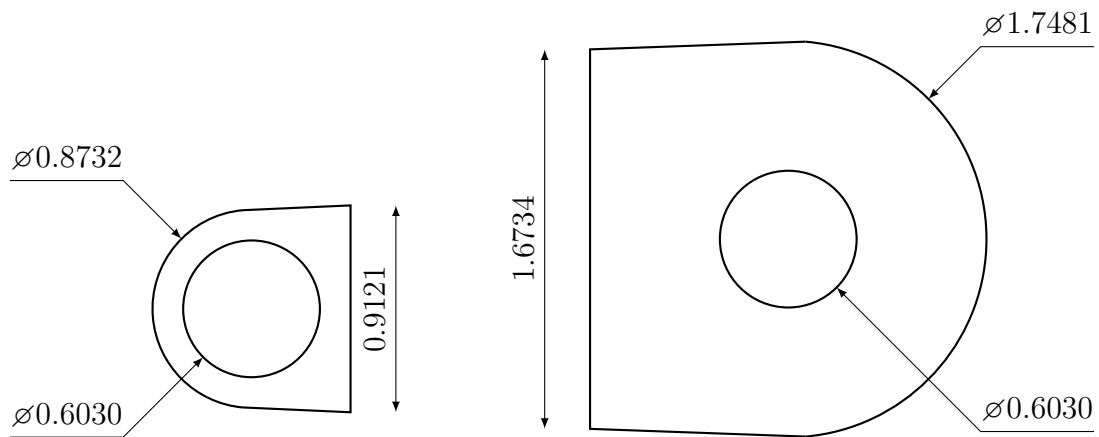


Fig. 3.12.: Top view of the connection between inlet and outlet port with needle tip –values in mm–.

Table 3.5.: Simulation results for hydraulic resistances.

Element	slope [kg/m <sup>7</sup> ]	y-intercept [kg/m <sup>4</sup> s]	$R^2$	Sol. time [min]
$\mathcal{R}''_{cid}(\text{nozzle})$	$6.3238 \times 10^{15}$	$2.3724 \times 10^9$	0.9991	36.00
$\mathcal{R}''_{cis}(\text{diffuser})$	$-1.4555 \times 10^{15}$	$1.7996 \times 10^9$	0.9854	47.63
$\mathcal{R}'_{cid}(\text{nozzle})$	$6.9617 \times 10^{13}$	$4.8001 \times 10^8$	0.9972	63.42
$\mathcal{R}'_{cod}(\text{nozzle})$				
$\mathcal{R}'_{cis}(\text{diffuser})$	$2.9499 \times 10^4$	$4.6798 \times 10^8$	0.9972	53.44
$\mathcal{R}'_{cos}(\text{diffuser})$				
$\mathcal{R}''_{cod}(\text{nozzle})$	$2.3938 \times 10^{16}$	$3.9103 \times 10^9$	0.9995	34.07
$\mathcal{R}''_{cos}(\text{diffuser})$	$-1.4602 \times 10^{15}$	$8.4165 \times 10^8$	0.9253	35.33
$\mathcal{R}'_{ind}(\text{nozzle})$	$1.8060 \times 10^{16}$	$1.3907 \times 10^{10}$	0.9985	63.82
$\mathcal{R}'_{ins}(\text{diffuser})$	$-1.0635 \times 10^{16}$	$1.3143 \times 10^{10}$	0.9984	48.17
$\mathcal{R}'_{ous}(\text{nozzle})$	$1.9342 \times 10^{16}$	$1.3953 \times 10^{10}$	0.9986	59.80
$\mathcal{R}'_{oud}(\text{diffuser})$	$-1.2039 \times 10^{16}$	$1.3116 \times 10^{10}$	0.9988	65.47
$\mathcal{R}''_{ind}(\text{sudden contraction})$	$1.2834 \times 10^7$	$6.4085 \times 10^8$	0.9988	222.95
$\mathcal{R}''_{ins}(\text{sudden enlargement})$	$5.2985 \times 10^{16}$	$1.7799 \times 10^9$	0.9985	12.98
$\mathcal{R}''_{oud}(\text{sudden contraction})$	$1.7857 \times 10^{16}$	$1.4074 \times 10^9$	0.9997	69.77
$\mathcal{R}''_{ous}(\text{sudden enlargement})$	$4.6857 \times 10^6$	$1.5674 \times 10^9$	0.9972	6.10
$\mathcal{R}'''_{ind}(\text{sudden enlargement})$				
$\mathcal{R}'''_{oud}(\text{sudden enlargement})$	$-8.2013 \times 10^{14}$	$5.6863 \times 10^8$	0.9999	35.37
$\mathcal{R}'''_{ins}(\text{sudden contraction})$				
$\mathcal{R}'''_{ous}(\text{sudden contraction})$	$1.0421 \times 10^{16}$	$1.0746 \times 10^9$	0.9998	31.20

**Notes:**

1. Parametric sweep from 225 to 675 mm<sup>3</sup>/s. Step size: 45 mm<sup>3</sup>/s.

**3.4.1 Inlet and Outlet water columns**

The model for the inlet and outlet water columns are open reservoirs, since both have the same cross-section area, following Eq. (2.51), we have:

$$\mathcal{C}_{iwc} = \mathcal{C}_{owc} = \frac{A_{pip}}{\rho g}, \quad (3.15)$$

where  $A_{pip}$  is the cross-sectional area of the pipette. Substituting its numerical value from Table. 3.1, we obtain:

$$\mathcal{C}_{iwc} = \mathcal{C}_{owc} = 6.9744 \times 10^{-10} \text{ m}^3\text{Pa}^{-1}, \quad (3.16)$$

To represent the initial height of the pipettes  $h_i = 15 \text{ cm}$ , an initial pressure –voltage– is to be set:

$$p_i = \rho g h_i = 1470 \text{ Pa} \quad (3.17)$$

### 3.5 Model simulation

Using the results from previous sections, the HECM is configured in Simulink® following Fig. 3.2, including variable resistors –Fig. 3.6– when required. Actual configured model is shown in Fig. 3.13 for reference.

Using this model, the pumped volume over time and characteristic curve are obtained, this curves will be validated in the next chapter.

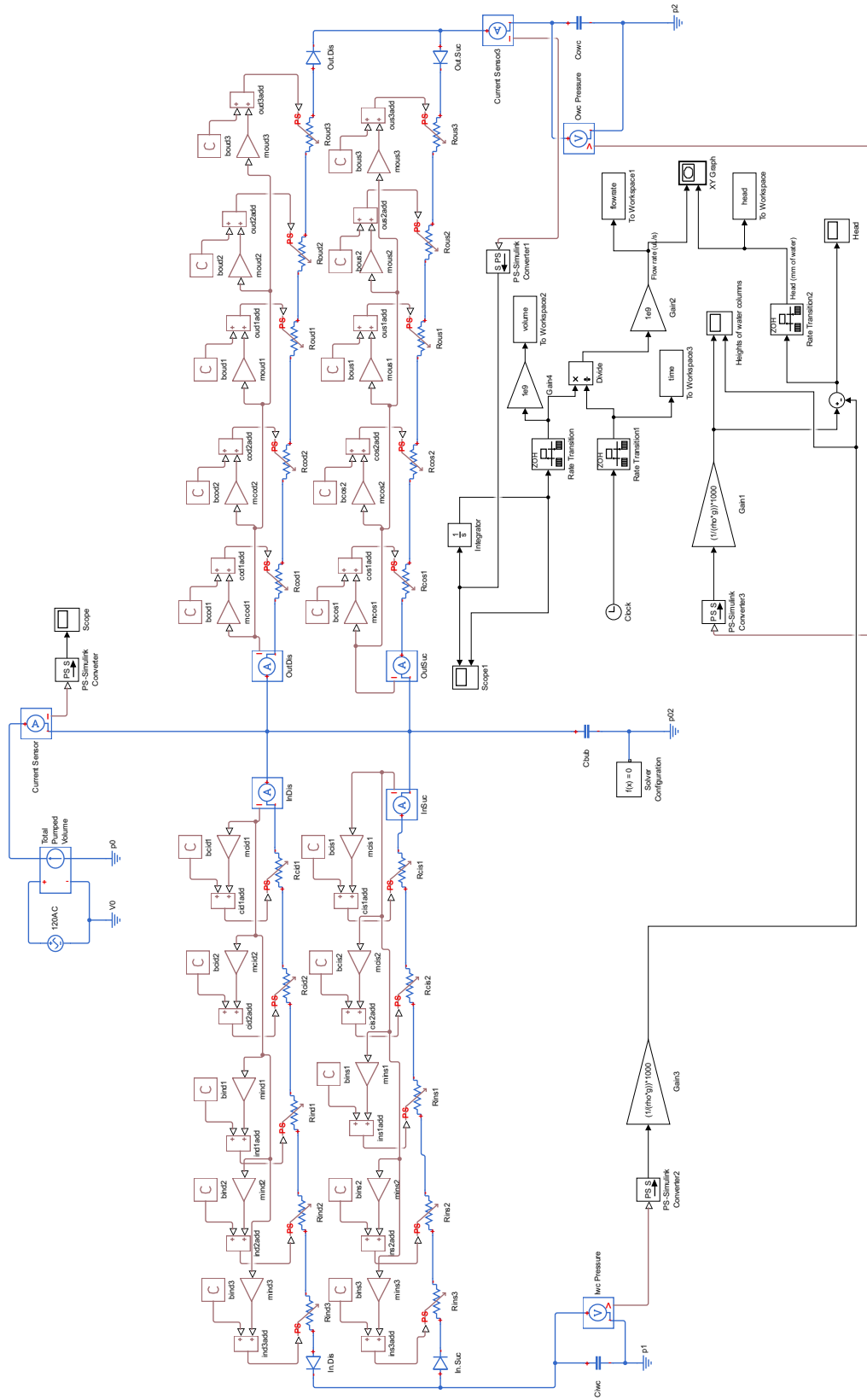


Fig. 3.13.: Implemented simulink model.

## 4. EQUIVALENT CIRCUIT MODEL VALIDATION

The HECM was validated using both a complete FEM simulation and a fabricated prototype. The configurations, steps and results of the FEM simulation are summarized in Section 4.1. Fabrication technique and results of fabricated prototype are shown in Section 4.2.

### 4.1 FEM Simulation

The simulation of the complete PVM was made using COMSOL Multiphysics <sup>®</sup> software, the following steps were taken –detailed information in Table 4.1–:

1. Geometry was defined as shown in Fig. 4.1. None of the adhesive materials, neither the top electrode film, were included in the analysis.
2. *Solid mechanics* and *electrostatics physics interfaces* were coupled using the *piezoelectric effect*.
3. A sinusoidal waveform  $V_f(t)$ , was defined with frequency  $f$ , and amplitude  $V_p$ . Its output is applied as the *electric potential* of the top electrode of PZT actuator. Bottom electrode is defined as *ground*.
4. A pressure  $p_{gs}$  is applied in positive  $z$  direction onto the downside boundary of the glass membrane.
5. A time-dependent study for *solid mechanics* and *electrostatics* is solved from 0 to 10T seconds with time step of T/20 seconds, deflection of membrane  $w_{gs}(r, t)$  is determined.
6. *Fluid structure interaction* and *solid mechanics physics interfaces* were coupled using  $w_{gs}(r, t)$  as *prescribe displacement* over the glass membrane.

7. The variable  $Q_i(t)$  is defined by means of an *integrator operator* applied in the inlet, and  $Q_o(t)$  is defined using an *integrator operator* applied in the outlet, in both cases the fluid velocity is the integrated variable, that is:

$$Q(t) = \iint_S \mathbf{u} \cdot \mathbf{n} dS \quad (4.1)$$

8. The variable  $\mathcal{V}_o(t)$  is defined using a *Global equation node* –an ODE– as follows:

$$\mathcal{V}_o(t) = \int Q(t) dt \Rightarrow \mathcal{V}'_o(t) - Q(t) = 0 \quad (4.2)$$

9. The pressure in the inlet  $p_{in}$  and outlet  $p_{ou}$  are defined a function of the variable  $\Delta h$ , as follows:

$$p_{in} = \rho g h_i - \Delta h/2 \quad p_{ou} = \rho g h_i + \Delta h/2 \quad (4.3)$$

10. A time-dependent study for *fluid structure interaction* is solved from 0 to 10T seconds with time step of T/20 seconds. To couple the deflection  $w_{gs}(r, t)$  calculated in the first study, the *values of variables not solved for* are taken from this study.

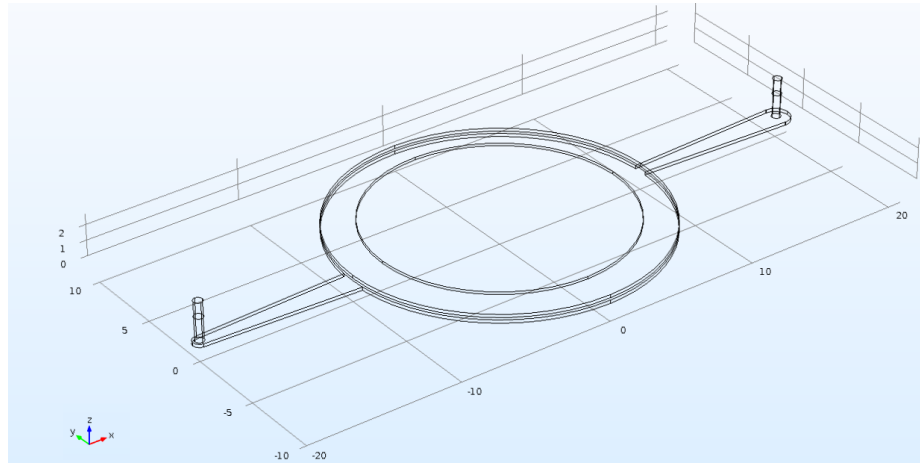


Fig. 4.1.: Geometry used in COMSOL for PVM.

If values of Table 4.2 are plotted, the characteristic curve of the simulated PVM is obtained as shown in Fig. 4.5.

Table 4.1.: Simulation configurations for complete PVM.

<b>Parameters</b>			
All parameters defined on Table 3.2, and additionally the following:			
<i>COMSOL name</i>	<i>Document symbol</i>	<i>COMSOL name</i>	<i>Document symbol</i>
ch.t	$t_{ch}$	deltah	$\Delta h$
<b>Ramp</b>			
<i>Name</i>	<i>Location</i>	<i>Slope</i>	<i>Cutoff</i>
rm1	0	f/2	1
<i>Smoothing</i>	<i>Transition zone</i>		
at cutoff	1/(4f)		
<b>Waveform</b>			
<i>Name</i>	<i>Type</i>	<i>Ang. freq.</i>	<i>Phase</i>
wv1	sine	omega	0
<i>Amplitude</i>			
Vp			
<b>Integration coupling</b>			
<i>COMSOL Name</i>	<i>Entity level</i>	<i>Applied in</i>	
intop1	boundary	inlet	
intop2	boundary	outlet	
<b>Variables</b>			
<i>COMSOL Name</i>	<i>Document symbol</i>	<i>COMSOL definition</i>	
Vpz	$V_f(t)$ (ramped)	rm1(t[1/s])*wv1(t[1/s])	
pressvar	$p_{gs}$ (ramped)	rm1(t[1/s])*press	
inflow	$Q_i(t)$	comp1.intop1(comp1.w_fluid)	
outflow	$Q_o(t)$	comp1.intop2(comp1.w_fluid)	
<b>ODE's –Global equations–</b>			
<i>COMSOL Name</i>	<i>Document symbol</i>	<i>COMSOL definition</i>	
vpump	$\mathcal{V}_o(t)$	vpumpt-outflow=0	

Table 4.2.: Simulation results for complete PVM.

<b>First study: Piezoelectric effect</b>		
$V_p$ [V]	<i>Highest deflection</i> [ $\mu\text{m}$ ]	<i>Sol. time</i> [min]
169.71	17.5	179.98
<b>Second study: Fluid structure interaction</b>		
$\Delta h$ [mm of water]	$Q(\Delta h)$ [ $\mu\text{L/s}$ ]	<i>Sol. time</i> [min]
0	9.3847	396.50
5	9.1522	240.88
10	8.2160	406.10
15	7.5475	249.30
20	7.3612	244.25
25	6.0440	287.46
30	5.7876	281.45
35	4.9643	339.80
40	4.8143	302.15
45	3.8516	179.88
50	2.4811	302.88
55	2.5375	390.92
60	1.5349	258.06
65	0.8124	261.27
70	-0.1776*	275.02
<b>Total solution time [hours]</b>		76.59

\* At this value of pressure head, the PVM is unable to deliver a positive flowrate

## 4.2 Fabricated prototype

A PVM was built using a low-cost fabrication technique. This technique was called GAG (glass-adhesive-glass). A picture of the fabricated prototype partially filled with coloured water is shown in Fig. 4.2.

The main motivation for the selection of the manufacturing process was to get a low-cost and repeatable fabrication technique. This was achieved through the GAG technique which uses a combination of glass and adhesive layers to create a flow path as shown in Fig. 2.1. In order to work as intended, one of the layers of glass needs to be very thin to have a wider range of elastic motion, thus exhibiting a typical membrane behavior when properly excited. The other piece of glass must be thicker for structural purposes. The thickness of the chosen adhesive sets the transversal area of flow. In this case the thicknesses of the glass layers were  $980\ \mu\text{m}$  and  $150\ \mu\text{m}$ , and  $205\ \mu\text{m}$  thick for the adhesive layer.

The general steps to produce a complete, functional micropump are described here:

1. The pump's design is cut onto an adhesive, using a computer controlled electronic cutting machine.
2. Two holes are drilled on the thick glass, with a position. coincident with the inlet and outlet of the design.
3. One side of the adhesive is then pressed onto the previously cleaned thick glass.
4. The thin glass –stored in clean and dry conditions– is placed over the reverse side of the adhesive, applying pressure.
5. A piezoelectric buzzer is glued to the thin glass, on the central position of the pump.

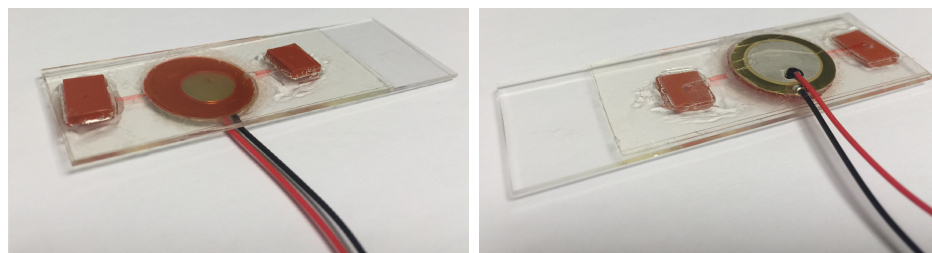


Fig. 4.2.: Fabricated prototype.

Once fabricated, an experimental setup was used in order to determine the head-flow characteristic curve of the micropump, a picture of the setup is shown in Fig. 4.3. The setup consist of:

- An aluminum main base with a rectangular shallow slot connected to an orifice drilled in the vertical aluminum flat bar. The slot was milled to successfully install the PVM with the piezoelectric buzzer facing down while the glass is supported in the main base.



Fig. 4.3.: Experimental setup with a prototype on place.

- A vertical aluminum flat bar connecting the main base with a raised base. An horizontal orifice is drilled in the flat bar to take the leads of the piezoelectric buzzer out of the setup for an easier connection to the source.
- A raised aluminum base –75 cm higher than the main base– with two vertical holes to allow the pipettes to go through.
- A 3D printed PLA base with two holes tighten to the pipettes with a double layer adhesive to fix it to the raised base.
- A simple start/stop –two buttons– control for the 120Vrms power supply.
- A camera programmed to take a picture every second.
- A timer to include the time when the picture was taken.

Using the described setup the displaced volume over time is measured and with this data, a flowrate  $Q(\Delta h)$  was calculated for each height, using Eq. (4.4). Data for a couple of the most representative tested PVM's is chosen. Prototype #1 was a PVM with low pressure head, it was chosen because it represents the worst case scenario. Prototype #2 represents the expected behavior of the PVM.

$$Q(\Delta h) = \frac{\mathcal{V}_{h_2} - \mathcal{V}_{h_1}}{t_{h_2} - t_{h_1}} \quad (4.4)$$

Plots of those results are shown in Fig.4.4 and 4.5.

The differences between the two selected PVMs can be explained by the following reasons:

- The relation between the diameter of the chamber –20 mm– and the width of the glass –25.4 mm– leave a little chance to fail, and centering becomes critical, some PVMs were not perfectly centered but were tested anyway.
- Double sided adhesive tape was not a chemical resistant product, its resistance to water and alcohol –used for cleaning and filling purposes– was not the best.

- Drilled hole for inlet and outlet was not a precision job, difference were evident in some of the fabricated prototypes.
- Glass thickness was not exactly equal all the times, some minor differences were encountered.
- Connection ports were made using a silicon adhesive backed square with a manually made hole in the center.

### 4.3 Results comparison and discussion

First, in terms of the pumped volume over time, we can see that there is no data from FEM simulation, this is due to the fact that it would be too costly, in terms of computation resources, to simulate the behavior of the PVM for 60 seconds or more, instead of that, the simulation was run just for ten periods –0.1667 seconds–, since it was clear that steady state was reached by that time. For this reasons Fig. 4.4 only shows data from the prototypes and the HECM simulation.

To construct the characteristic curve using FEM simulations, it was necessary to solve a simulation for every data point in the plot, results are summarized in Table 4.2. For the HECM, the data is obtained directly from the simulation. In the case of the prototypes Eq. (4.4) was applied to obtain the curve.

As shown in Fig. 4.5, FEM simulation results are almost linear, and always higher than the experimental results and the HECM, this can be due to many factors:

- Deflection of the membrane is calculated with a constant counter-pressure of 15 mm of water, but is important to clarify that membrane deflection used to determined the flow source included in the HECM is calculated with the same constant counter-pressure.
- A water bubble is not included in FEM simulations because it will dramatically increase the complexity of the model, since it would require the use of two-phase flow. In all experiments, water bubbles were present.

- The transition between the pipette diameter to the needle diameter was not included in the model, because it will increase in more than double the mesh elements to be solved.

To analyze Fig 4.5 in a quantitative way, two statistic indicators were used, the *coefficient of determination*  $R^2$  and the average of the percentage of difference between data points using a reference, in this case, the two prototypes. Results are shown in Table 4.3. A qualitative comparison between the two modeling approaches is shown in Table 4.5.

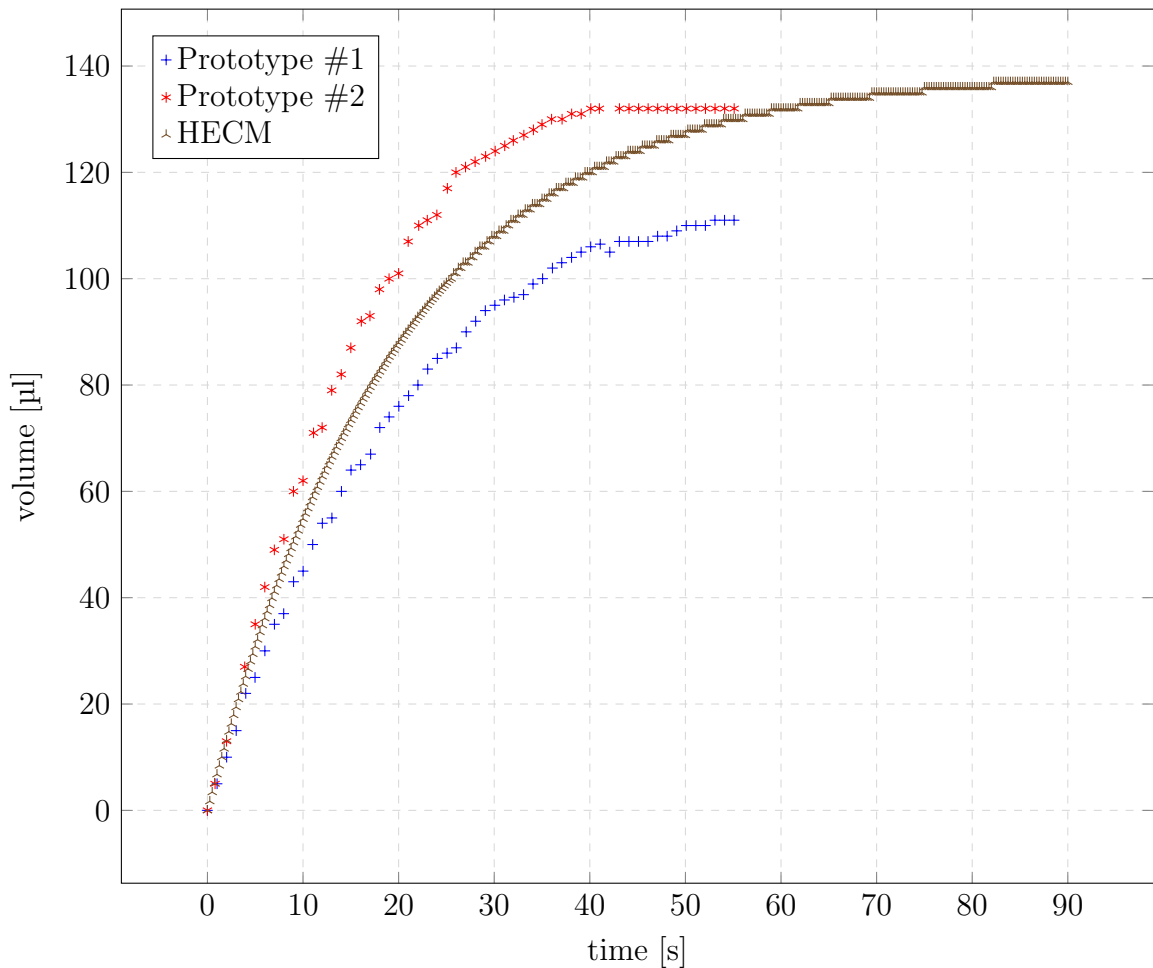


Fig. 4.4.: Pumped volume over time

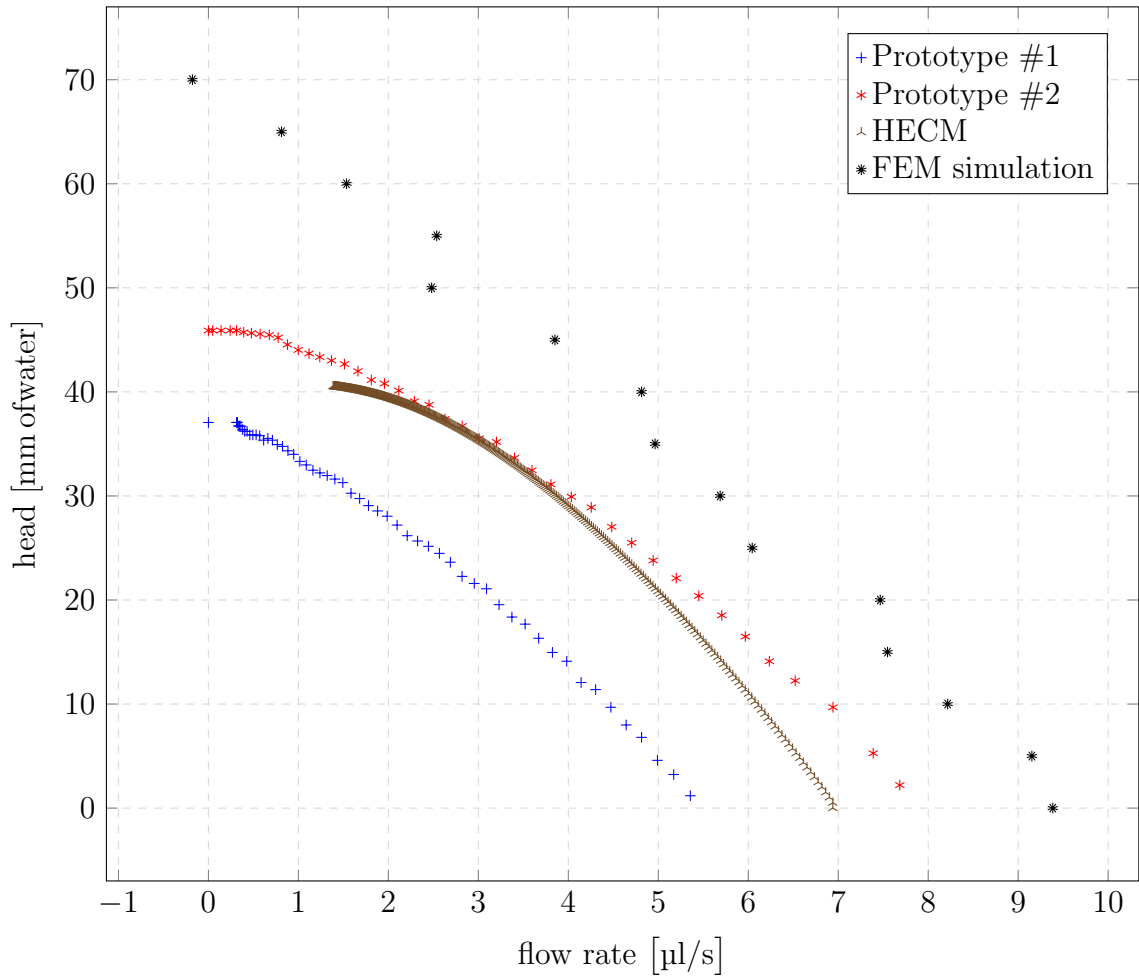


Fig. 4.5.: Characteristic curve of PVM

As shown in Table 4.4, the HECM is almost 5 times faster to be solved than the complete FEM simulation and configuration time is much lower. It is important to emphasize that, the HECM is not only faster, but also offer the capability of changing some of the elements without recalculating everything. In contrast, any change in the FEM simulation will require to run the complete set of simulations again.

Table 4.3.: Quantitative comparison.

<i>Data set</i>	<i>Range</i> [ $\mu\text{L/s}$ ]	$R^2$	<i>Average difference</i> [ %]
<b>Reference: Prototype #1</b>			
HECM	1.4 – 5.4	0.9865	173.20
FEM Sim.	0 – 5.4	0.9927	278.90
<b>Reference: Prototype #2</b>			
HECM	1.4 – 6.9	0.9941	16.00
FEM Sim.	0 – 7.9	0.9846	94.60

Table 4.4.: Solution time comparison.

<i>Description</i>	<i>Solution time</i> [min]
<b>HECM</b>	
Actuator axisymmetric simulation	0.78
Simulation for hydraulic resistance determination.	885.51
Simulink simulation	0.50
Configuration time –approximate–	400.00
TOTAL [hours]	21.45
<b>FEM Simulation</b>	
Actuator simulation	179.98
Flow simulation at different pressure heads	4415.92
Configuration time –approximate–	1800.00
TOTAL [hours]	106.60

Table 4.5.: Qualitative comparison for the PVM .

Characteristic	HECM	FEM Simulation
All elements are included	yes	no
Include water bubble	yes	no
Solution time	lower	higher
Individual elements give flexibility	yes	no
Agreement with experimental results	fair*	poor
Convergence problems in FEM simulations	minimal	very high
Mesh complexity in FEM simulations models	low	very high

\*Agreement of 16% obtained with Prototype #2

## 5. CONCLUSION AND OUTLOOK

### 5.1 Conclusion

This thesis has demonstrated the applicability and the advantages of a HECM over a complete FEM simulation for characterizing a PVM.

A HECM of the PVM was developed using lumped elements, each element was chosen using the analogies between electrical and fluidic systems, and characterization of the elements was done easily. Once all the network were built, the parameters of the HECM lumped elements were successfully determined by means of analytical solutions in some cases and in other cases by FEM simulations. The simplicity of the elements of the HECM that were simulated using FEM software helped to avoid convergence problems.

A complete FEM simulation of the PVM was configured and solved, it was a complex task to solve many convergence problems encountered during the process. Coupling between three different physics –including a one-way coupling– were successfully achieved.

A set of fully functional prototypes were fabricated using a low-cost fabrication technique called *GAG*, an experimental setting was prepared and time-volume and flowrate-head curves were obtained, data from two prototypes were used.

Using experimental data, the HECM and the FEM simulation were assessed and compared. The HECM was 5 times faster in obtaining the required results and it was more accurate to describe the behavior of the PVM.

The main contribution of this work was to demonstrate that is better to construct a systemic approach first –using conventional system models– and then determine the behavior of the components of the system using the best approach for each case, than build a complete model in FEM software and solve it at full complexity.

## 5.2 Outlook

The HECM parameter determination techniques developed in this work can be studied in a broader and deeper way, relation between hydraulic resistances calculated by FEM simulation and their correspondent analytic theories were not explored in this work.

A determination of the behavior of pressure drop in *accessories*, commonly known as *minor losses* in macroscale fluid mechanics in laminar flow condition in the microscale –not nanoscale– will be very useful for future developments in this area of research.

The used fabrication technique can be improved in many ways, a better and wider double layer adhesive is vital for future experiments. A wider base and membrane glass is also very important. Experiments with a smaller piezoelectric buzzer are necessary for future development. In general, the low-cost PVM fabrication using the *GAG* technique offers many opportunities for undergraduate research.

## REFERENCES

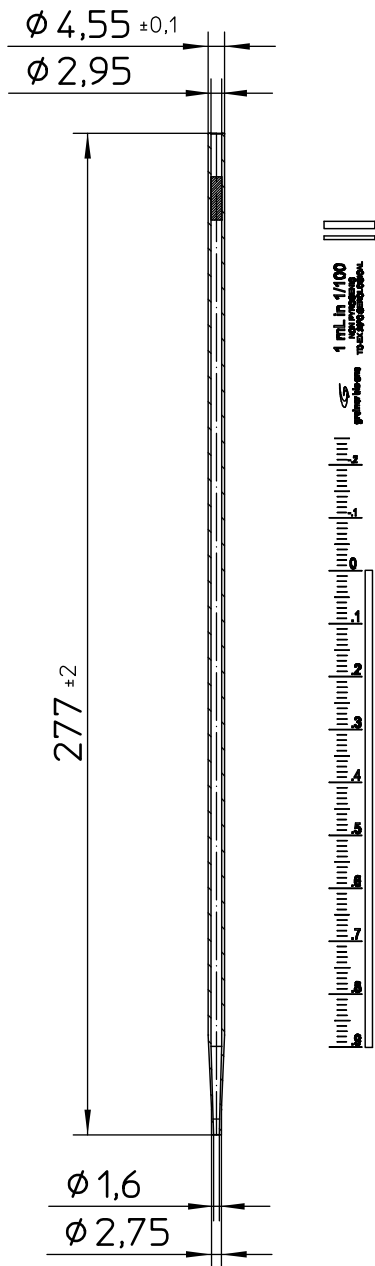
## REFERENCES

- [1] W. C. Young and R. G. Budynas, *Roark's formulas for stress and strain*. McGraw-Hill, 2002, vol. 7.
- [2] T. Papanastasiou, G. Georgiou, and A. N. Alexandrou, *Viscous fluid flow*. CRC Press, 1999.
- [3] J. A. Pelesko and D. H. Bernstein, *Modeling Memes and Nems*. CRC press, 2002.
- [4] Crane Co, *Flow of Fluids Through Valves, Fittings and Pipes*. Crane Co., 1972, no. 410.
- [5] Y. A. Cengel and J. M. Cimbala, *Fluid mechanics*. McGraw Hill, Boston, MA, 2006.
- [6] H. Bruus, *Theoretical Microfluidics*. Oxford University Press, Oxford, 2008.
- [7] S. Das, *Mechatronic modeling and simulation using bond graphs*. CRC Press, 2009.
- [8] V. M. Alfaro, "Modelado y análisis de los sistemas dinámicos utilizando la red generalizada," *Universidad de Costa Rica*, 2005.
- [9] H. M. Paynter, *Analysis and design of engineering systems*. MIT press, 1961.
- [10] V. M. Alfaro, "La red generalizada, teoremas y propiedades," *Universidad Tecnológica de Panamá*, 1986.
- [11] K. Ogata, *System dynamics*. Prentice Hall New Jersey, 2004, vol. 4.
- [12] N. S. Nise, *Control Systems Engineering*. John Wiley & Sons, 2007.
- [13] V. M. Alfaro, "La red generalizada," *Revista Ingeniería-Engineering Research*, vol. 1, no. 2, 1991.

## APPENDICES

## A. DATASHEETS

Valid for Item-No.: 604107, 604160, 604181, 606160-TRI



"All dimensions in mm"

Customer drawing subject to change without notice!

Uncontrolled Copy

Prior Issue	Drawn	Approved	Released	CONFIDENTIAL: Information contained in this document or drawing is confidential and proprietary to Greiner Bio-One GmbH. This document may not be reproduced for any reason without written permission from Greiner Bio-One GmbH. All rights of design, invention, and copyright are reserved.
Revision 2	Date 2011/05/10	Date 2015/12/10	Date 2015/12/10	
Date 2013/05/21	Name forb	Name forb	Name sonntag	



Part No: CEB-20D64

Date: 7/28/2006

Unit: mm

Description: piezo electric diaphragm

Page No: 1 of 4

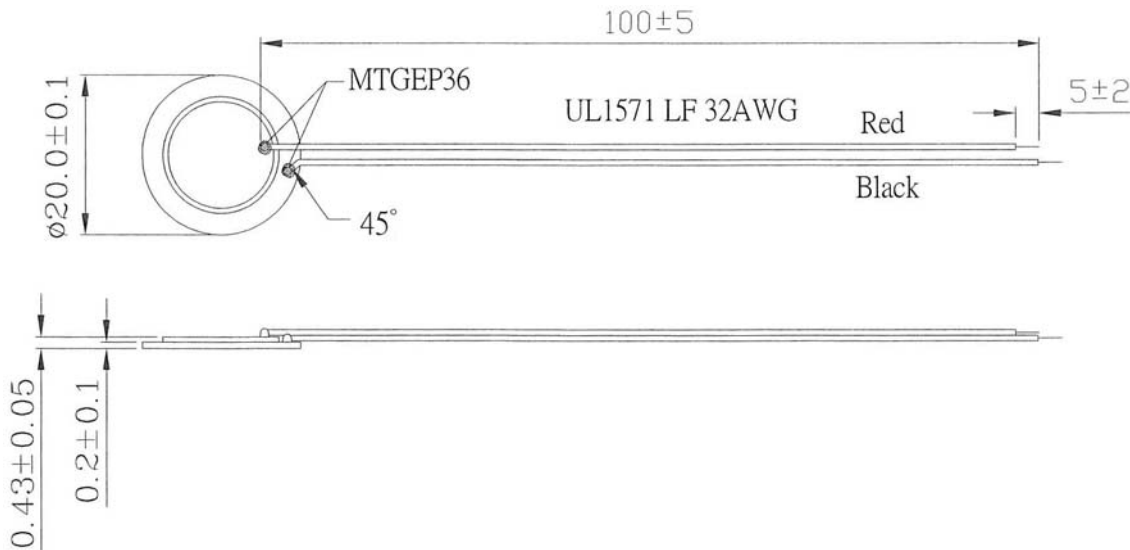


### Specifications

Maximum input voltage	30 Vp-p	
Resonant frequency	6.5 ± 0.5 KHz	see Measurement Methods
Resonant impedance	350 Ω max.	see Measurement Methods
Electrostatic capacitance	13,000 ±30% pF	at 120 Hz / 1 V
Operating temperature	-20 ~ +70° C	
Storage temperature	-30 ~ +80° C	
Dimensions	Ø20.0 x H0.43 mm	
Weight	1.50 g max.	
Material	Brass	
Terminal	Wire type	
DC resistance	20 M Ω min.	Fluke 45 rate: Fast Measurement time: 1 second (only for ≤ 20 mm test)
RoHS	yes	

### Appearance Drawing

Tolerance: ±0.5



## Cover glass specifications



### **BSR/VR** Fisherbrand™ Cover Glasses: Rectangles

Made of finest optical borosilicate glass, with uniform thickness and size

Glass, Cover; Fisherbrand; Microscope; Rectangles; Optical borosilicate glass; Uniform thickness and size; Corrosion resistant; Lint-free; Rectangles No. 1 to 0.13 to 0.17mm thick; Size: 60 x 24mm

[View all options for this product](#)

Catalog No. 12-545M

● **\$18.63 / Pack**

~~\$37.25 / Pack~~

**Online Savings (50%)**

○ **\$157.49 / Case of 10 PK**

~~\$314.97 / Case of 10 PK~~

**Online Savings (50%)**

Qty  [Check Availability](#)

**Add to Cart**

### Description & Specifications

Rectangular shape.

- Corrosion-resistant
- Lint-free and ready to use

### Specifications

Material	Borosilicate Glass
Shape	Rectangular
Length (Metric)	60mm
Width (Metric)	24mm
Thickness (Metric)	0.13 to 0.17mm
For Use With	Microscope, histology, cytology, hematology, microbiology
Product Type	Coverglass

## Microscope slides specifications

Your Shopping Basket 0 Item(s) \$0.00

[home](#) | [contact](#) | [privacy](#) | [email](#) | [site map](#) | [view cart](#)



SEARCH

[Chang Bioscience, Inc.](#)  
[Anatomical model](#)  
[Anatomy Guide](#)  
[Glassware & Plasticware](#)  
[Microscope & slide](#)  
[Lab Equipment](#)

E-COMMERCE BY 

[Home](#) > [Microscope & slide](#) > [Slide & Cover Slip](#) > Slide cover glass 22 \* 50 mm 100 pcs

### Slide cover glass 22 \* 50 mm 100 pcs



Item# C2250\_1  
**Regular price: \$3.79**  
**Sale price: \$3.29, 5/\$14.49**

#### Product Description

1 box 100 pcs  
22 x 50 mm  
0.13-0.17 mm thick

[HOME](#) | [CONTACT](#) | [PRIVACY](#) | [EMAIL](#) | [SITE MAP](#) | [VIEW CART](#)

Copyright 2009 Chang Bioscience, Inc. All rights reserved.